Chiral resonators: Selected electromagnetic and optomechanic applications in microwave and plasmonics

by

Aybike Ural Yalçın

A Dissertation Submitted to the
Graduate School of Sciences and Engineering
in Partial Fulfillment of the Requirements for
the Degree of

Doctor of Philosophy

in

Physics

KOÇ UNIVERSITY

February, 2018

Chiral resonators: Selected electromagnetic and optomechanic applications in microwave and plasmonics

Koç University

Graduate School of Sciences and Engineering

This is to certify that I have examined this copy of a doctoral dissertation by

Aybike Ural Yalçın

and have found that it is complete and satisfactory in all respects,

and that any and all revisions required by the final

examining committee have been made.

Committee Members:

Assoc. Prof. Kaan Güven

Prof. Ali Serpengüzel

Prof. İrşadi Aksun

Assoc. Prof. Hakan Özgür Özer

Assoc. Prof. Ahmet Levent Subaşı

Date:

To my family and my cats

ABSTRACT

This thesis investigates selected electromagnetic and optomechanic properties of chiral resonator structures in the microwave and plasmonic (optic) regime, respectively.

The first part of the thesis focuses on the systematic study of the electromagnetic response of canonical spiral shaped chiral resonators in the microwave regime. Canonical spiral provides a chiral extension of the split ring resonator which is a well-known building element of the electromagnetic metamaterials. Various configurations of single and coupled chiral resonators are studied experimentally and computationally. In particular, the role of chirality in coupled configurations consisting of same-handed and opposite handed (enantiomeric) canonical spirals is investigated. Within a waveguide one-dimensional periodic arrays of canonical spirals with same or alternating handedness, that give rise to chirality-dependent band gaps within the transmission band of the fundamental mode of the waveguide are constructed. Based on a good agreement between experiments and simulations the following results are prominent: (i) optimal canonical spirals are fabricated which exhibit both electric and magnetic dipole excitation at the same resonance frequency. (ii) resonance splitting of coupled spirals show that the lower (higher) mode is stronger for spiral pairs of same (opposite) handedness. (iii) chains of spiral pairs exhibit chirality selective stop bands respectively at the lower and upper frequency modes of an individual spiral pair. A chain with uniform helicity opens a gap at the high frequency mode whereas a chain consisting of enantiomer pairs opens a gap at the lower frequency mode.

The second study involves the optomechanical effects of canonical spiral chiral plasmonic resonators which can be utilized for chirality selective optical trapping and binding functionalities. The spectra of the optical force components that act on a

single or coupled spiral system under plane-wave excitation are computed. We then repeat the calculations in the presence of a planar metal surface in the vicinity of the spirals. This study is based on a theoretical and computational (simulation-based) framework. The major outcomes of this part are that for spiral pair the relative lateral force perpendicular to the incident polarization direction are chirality dependent. The same handed spiral pair tends to bind by an attractive force, whereas the opposite handed pair repel each other. The optical force acting in the direction of the light propagation on the single or coupled spiral pair is independent of the chirality. The presence of the metal substrate generates a strong attractive force towards the metal surface on the spiral resonators.

ÖZETÇE

Bu tez, kiral bir rezonatör yapısının mikrodalga ve plazmonik (optik) dalgaboylarındaki seçilmiş elektromanyetik ve optomekanik özelliklerinin araştırılması üzerine yapılmıştır. Tezin birinci bölümü, kanonik sarmal adlandırılan kiral bir rezonatör yapısının mikrodalga C-bandında (5-8 GHz) elektromanyetik tepkilerini sistematik araştırılmasından oluşmaktadır. Kanonik sarmal, elektromanyetik metamalzemelerde temel yapı taşı olan yarıklı halka rezonatörlerinin kiral bir uzantısı olarak en basit sarmal yapıdır. Kanonik sarmal yapının tekli ve çiftli olarak farklı konfigürasyonlarının elektromanyetik tepkisi, deneysel ve sayısal olarak çalışılmıştır. Özellikle çift yapıların eş ya da zıt kiral sarmallardan oluşmasına göre elektromanyetik tepkinin nasıl ve neden değiştiği üzerinde durulmuştur. Bunu takiben, eş ya da zıt kiral sarmal çiftlerinin doğrusal evresel sıralanmasıyla oluşan zincir yapılar dalga kılavuzu içine konularak, dalga kılavuzunun geçirgenlik bandında oluşan kiral bağımlı yasak bantların oluşumu incelenmiştir. Deney ve simülasyonlardaki iyi uyuma dayanarak aşağıdaki bulgular vurgulanmaktadır: (i) Aynı frekansta elektrik ve manyetik uyarılma gösteren optimal kanonik sarmal yapılar tasarlanmış ve üretilmiştir. (ii) Çiftli yapıların gösterdiği rezonansın iki farklı moda ayrılması durumunda baskın rezonansın eş (zıt) sarmal çiftlerinde düşük (yüksek) frekansta oluştuğu gösterilmiştir. (iii) Kanonik sarmal çiftlerinden oluşan zincirlerin, tek bir sarmal çiftin iki farklı mod frekansında yasak bantlar oluşturdugu gösterilmiştir. Bu yasak bantlar, çiftler arası etkileşen sarmallar aynı kiral yapıda olduğunda yüksek frekans bandında, zıt kiral yapıda olduğunda düşük frekans bandında baskın hale gelmektedirler.

Tezin ikinci bölümü optik dalgaboylarında plazmonik rezonans davranışı gsteren kanonik sarmallara etkiyen optik kuvvetlerin araştırılmasını kapsamaktadır. Bu kuvvetlerin kiral seçici optik tuzaklama ve optomekanik bağ oluşturma uygulamaları olabilir.

Bu kapsamda, tek ve çift sarmal yapılarında doğrusal polarizasyonda ışık uyarılması altında oluşan optik kuvvetin bileşenleri hesaplanmıştır. Bu hesaplar sarmallarn altında düz metal bir yüzey olması durumu için tekrarlanmıştır. Bu çalışmalar kuramsal ve sayısal metotlarla gerçekleştirilmiştir. Çalışmanın ana bulguları, sarmal çifti yapılarında polarizasyona dik yanal yöndeki bağıl kuvvetin kiral seçici olduğunu göstermiştir: Buna göre zıt kiral sarmal çiftleri çekici kuvvet ile bağlanırken, eş kiral çiftleri zıt kuvvet ile birbirini itmektedir. Uyarıcı ışığın yayılımı yönünde tekli veya çift sarmal yapıya etkiyen kuvvet kiral özelliklerinden bağımsız bulunmuştur. Metal yüzeyin varlığı, sarmal rezonatör yapılar için yüzeye doğru güçlü bir çekici kuvvet oluşturmaktadır.

ACKNOWLEDGMENTS

First of all, I would like to thank my supervisor Assoc. Prof. Kaan Güven whose encouragement, guidance and support from the initial to the final level enabled me to develop an understanding of my research work. During thesis work, his great efforts to explain things clearly and simply significantly helped me to understand and develop the work presented. And, I also acknowledge for his endeavor and patience to gain my motivation at crucial moments.

I would like to thank to my thesis committee member Prof. Ali Serpengüzel, Prof. İrşadi Aksun for their advice, suggestions throughout my Ph.D. study.

I would like to thank my thesis committee members Assoc. Prof. Levent Subaşı, Assoc. Prof. Hakan Özgür Özer for their patience and tolerance.

The department of Physics of Koç University, has provided an excellent professional environment for every researcher where any kind of financial, technical, or mental support is unexceptional. I would like to thank all the academic and the administrative personel of Koç University. I acknowledge TUBITAK for providing me the scholarship under the national graduate scholarship program supporting the research and my graduate study.

I would like to thank my family, but especially my granduncle and my grandaunt for their mentorship and suggestions for my career. Also I am grateful to my mother for supporting me in every sense. Last but not least, I would like to thank my husband for always being with me, encouraging, supporting, and tolerating me during my doctoral studies.

TABLE OF CONTENTS

LIST OF FIGURES

Chapter 1

INTRODUCTION

The chirality refers to a structural property of an object that cannot be superimposed on its mirror image as it is first introduced by Lord Kelvin [1]. The word chirality originates from the Greek word "$\chi\varepsilon\iota\rho$" (kheir) which means hand. At macro scale our hands, shell of snails are chiral, at molecular scale proteins, sugar are examples of the chirality in nature. To this end, light (i.e. electromagnetic waves) can also be chiral, when the polarization vector rotates "left" or "right" with respect to the propagation axis. Chiral medium produces optical activity such as polarization rotation, circular dichroism since a chiral medium responds differently to left and right circularly polarized light. The first observation of polarization rotation was through natural chiral material quartz discovered by F.J.Arago [2]. Materials with strong optical activity meet the need as polarization controller, circular polarizers for optoelectronic, imaging and display applications and are also in photography [3]. The optical activity in a chiral media is induced by electro-magnetic coupling. The possibility of designing materials with higher electro-magnetic coupling with increased chirality parameter lead to acquire giant optically active metamaterials[3]. Basically metamaterials are composed of periodically arranged resonant elements which exhibit unusual electromagnetic and optical properties, such as negative refraction, which are not seen in naturally occuring materials. The negative refraction is taken much attention because of its capability of constructing perfect lens [4]. This intringuing property is achieved by the combination of split ring resonators with metallic wires in microwave [5]. Chiral metamaterials show the possibility of realizing negative refraction by the use of chirality [6]. The manifestation of the strong optical activity and even negative refraction in chiral metamaterials are proposed in ref. [7, 8]. Various chiral resonators are used to build chiral metamaterials such as helical wires, chiral split ring resonators (SRR)[10], gammadions[9] or cross-wire[11] structures. The optical properties of chiral metamaterials is also studied in terahertz regime [12, 13, 14, 15]. Some designs are proposed to avoid bianisotropic effects [16, 17]. Omega shaped particles are also of interest as building blocks of metamaterials[18].The negative index metamaterial composed of omega shaped resonator arrays is experimentally verified [19, 20]. Transmission properties of metamaterials formed by omega shaped inclusions are investigated in ref. [21]. It is shown that the periodic arrays result in band gaps due to the magnetoelectric resonances. Further, by designing the composite metamaterial, a transmission band is opened. Another artificial chiral object is a canonical spiral firstly suggested to replace to a small helix in order to simplify the electromagnetic analysis[22]. In ref. [23], an analytical antenna model is used to analyze such chiral scatterers. The canonical spiral is designed for chiral metamaterials where a circularly polarized wave is radiated for any linear polarization of the incident wave by Tretyakov et.al.[24]. This response is obtained by the optimal design of the canonical spiral. Another consequence of the optimal spiral is that a particular helicity is completely transparent for circular electromagnetic waves of the same helicity [24]. The canonical spiral with optimal design parameters is employed in cloaking application [25].

Light can exert radiation pressure on the object that it encounters and that resulting optical force can be used to manipulate particles. The gradient and scattering components of the optical forces are reported by Ashkin et al. on micron sized particles in 1970 [26] and the first demonstration of an optical tweezer for stable control of particles in free space given in [27]. The contribution of emerging field of plasmonics can not be neglected in calculations of optical forces on conducting particles. Optical forces become significant due to field enhancement near the structures as metal spheres, cylinders at their surface plasmon resonances [28, 29, 30, 31], and also for the gold nanospheres or nanorods which are coupled to a gold slab [32, 33]. Optical forces are utilized growingly in biomedical, chemical applications[34]. In biological studies, optical forces demonstrate themselves as optical tweezers which have a significant role to investigate the properties of DNA, proteins, cells. The importance of the optical forces reveals at sensitive identification and seperation of the enantiomers[35] in the field of drug research, pharmaceutical applications[36]. During the drug synthesis, while one of the enantiomer is harmless to human health, the other type could be detrimental[37]. Two types of optical forces can be mentioned that act on a chiral nanoparticle when an external electromagnetic field is incident, an achiral force and chiral one whose directions are opposite for nanoparticles of different handednesses. Chirality dependent forces could be even pulling as predicted in ref. [38]. In order to distinguish the enantiomers, the chiral fields should interact with the chiral structure. The chiral fields generations can be achieved by utilizing achiral resonator such as double split ring resonator [39]. In that case, magneto-electric coupling results in enhanced optical chirality that enables to seperate the enantiomers near plasmonically excited achiral resonators. Selective trapping of enantiomers are also shown by using coaxial plasmonic apertures [40]. The electromagnetic response of the chiral materials gives the chance to use optical forces for passive seperation[41, 42]. Another mechanism for chirality sorting is proposed by Capasso et. al. in ref. [43]. Chiral particles are subject to lateral optical forces which arise from the transverse component of the spin angular momentum (SAM) of evanescent waves [44], and those lateral forces are acting in a direction other than the gradient and scattering force directions. So chiral particles with different helicity will move in lateral opposite directions. Recently, Wang and Chan reported a lateral optical force on a chiral particle above a substrate by an electromagnetic plane wave [45]. This lateral force, which deflect the opposite handed particle in opposite directions, emerges as the particle interacts with the reflection of its scattered field. The chirality of the particle is coupled to both the lateral linear momentum and SAM generated by the scattered wave of the chiral particle above the substrate.

This thesis work contains two main sections as follows. The first part of thesis focuses on the systematic study of the electromagnetic response of canonical spiral shaped chiral resonators in the microwave regime. The single and coupled chiral resonators are examined in various configurations both experimentally and computationally. In particular the role of chirality in coupled configurations is studied based on same-handed and opposite handed (enantiomeric) canonical spirals. Furthermore, one-dimensional periodic arrays of canonical spirals with same or alternating handedness within a waveguide are constructed, that give rise to chirality-dependent band gaps within the transmission band of the fundamental mode of the waveguide.

The second study includes the optomechanical effects of canonical spiral chiral plasmonic resonators. The spectra of the optical force components that act on a single or coupled spiral system under plane-wave excitation are computed. Then the calculations are repeated in the presence of a planar metal surface in the vicinity of the spirals. This study is based on a theoretical and computational (simulation-based) framework.

Chapter 2

MICROWAVE RESONANCES OF SINGLE AND COUPLED CANONICAL SPIRALS

2.1 *Canonical spiral*

The canonical spiral resonator consists of a split loop with two perpendicular straight-wire sections connected to the edges of the gap. The geometry was proposed as an approximation to single true helix showing the same optimal properties under the linear excitation studied in ref.[24]. Based on the result of that study, we designed a canonical spiral with a resonance at about 7 GHz. Due to its chiral structure, the canonical spiral exhibits electric and magnetic coupling to a linearly polarized excitation under various spatial orientations. In order to investigate these couplings systematically we set up a configurational labeling depicted in fig. 2.1. These are as follows:

- Rods of canonical spiral parallel to the excitation wavevector: spiral loop gap (A) symmetric or (B) asymmetric with respect to the electric field,
- Rods of canonical spiral parallel to the electric field: spiral loop gap (C) symmetric or (D) asymmetric with respect to the excitation wavevector,
- Rods of canonical spiral parallel to the magnetic field: spiral loop gap (E) asymmetric or (F) symmetric with respect to the electric field.

The spiral loop radius is $r = 2.3$ mm, minor radius is $r_0 = 0.4$ mm, length of the straight arms is $l = 2.5$ mm as shown in Fig. 2.2. The minor radius is chosen to match the wire used in experiments. The gap distance of the loop is $g = 0.86$ mm. These

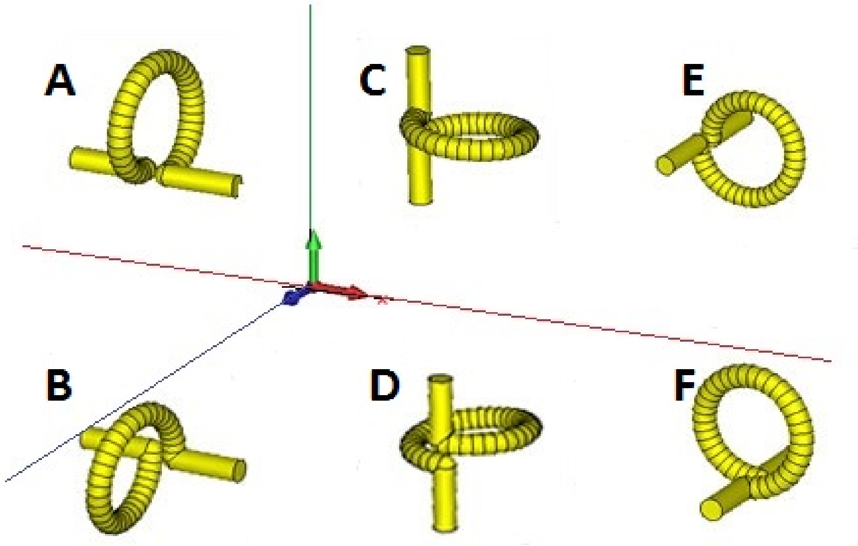

Figure 2.1: The six possible orientations A-F are shown in given coordinate system. The electric field polarized along y (green axis) direction, propagation is along x (red axis) direction.

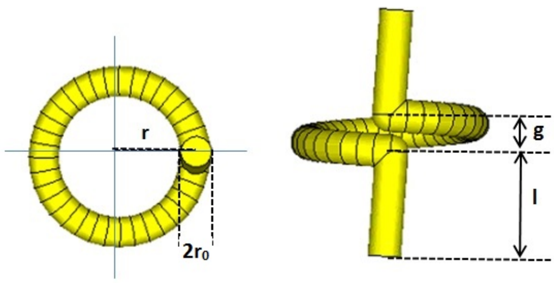

Figure 2.2: The radius of the spiral from the loop center to the center of the wire, $r = 2.3$ mm, the thickness of the wire $2r_0 = 0.8$ mm, length of the wire $l = 2.5$ mm and the gap $g = 0.86$ mm are shown.

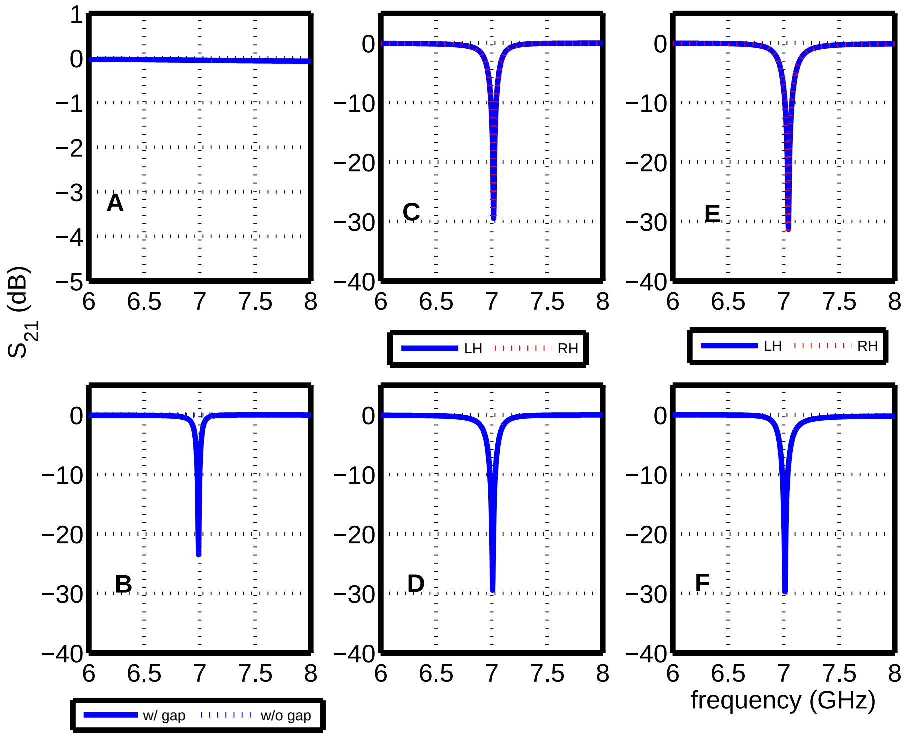

Figure 2.3: The transmission spectrum of the canonical spiral with left helicity (solid blue) and with right helicity (dashed red) within a rectangular waveguide, corresponding to the orientations depicted in Fig. 2.3. In (A), the spiral does not couple to the incident wave. This contrasts the orientation in (B) where the asymmetric positioning of the gap induces an electric coupling. C and D correspond to the electric coupling and E and F correspond to the magnetic coupling. Closing the gap destroys the resonance as shown by dotted line.

parameters provide an optimal response in which the resonance frequency is independent of incident polarization. The numerical calculations are done in Microwave Studio (CST), and the material is set to be copper. The resonance of the single spiral is analyzed inside a rectangular waveguide. PEC and PMC boundary conditions are imposed in the transverse (y and z) directions, respectively; the ports are defined such that the propagation direction is along the x axis. The transmission (S_{21}) spectrum is obtained by the frequency domain solver with an excitation pulse covering a relevant frequency band of 6-8 GHz.

Fig. 2.3 shows the electromagnetic response of the canonical spiral in six orientations depicted in Fig. 2.1 . In five of these orientations (B-F), a resonance is excited at 7.04 GHz. The orientation A corresponds to a dark state in which the spiral does not couple to the incident wave. Note that the gap is symmetric with respect to the polarization. When the gap becomes asymmetric (as in B), an electric coupling still induces the resonance. The orientations C and E can be interpreted as the spiral kept fixed in space and the imposed boundary conditions are reversed. In that case, the incident polarization can be defined as transverse electric (TE) and transeverse magnetic (TM), hence the canonical spiral has a resonance frequency independent of the polarization similar to that studied in ref [24]. We further verify that the resonance occurs due to the presence of the gap by calculating the response of a gapless canonical spiral which lacks any resonance in this frequency range [46, 23].

Fig. 2.4 shows the experimental spectrum corresponding to the six orientations of the canonical spiral given in Fig. 2.1. One to one comparison of Fig. 2.3 and Fig. 2.4 panels show a good agreement between the simulated and measured electromagnetic response. The resonances due to magnetic excitations are weaker as shown in Fig. 2.4.E-F.

The measurement of the electromagnetic spectrum of the spirals are performed with an Agilent 8719ES network analyzer and two WR137 5.85 - 8.20GHz (C-band) rectangular waveguides attached through coaxial SMA cables. Fig. 2.5 shows the photograph of a typical measurement setup. The canonical spirals are manufactured manually by using soldering wire. Photograph of the canonical spirals of left and right helicity is shown in Fig. 2.5. Note that the canonical spiral dimensions are of the order of lambda/7, rendering them as subwavelength resonators.

This section concludes that optimal spiral with polarization independent resonance at microwave is constructed experimentally bearing a good agreement to simulation results. The next section discusses the electromagnetic response of coupled spiral pairs.

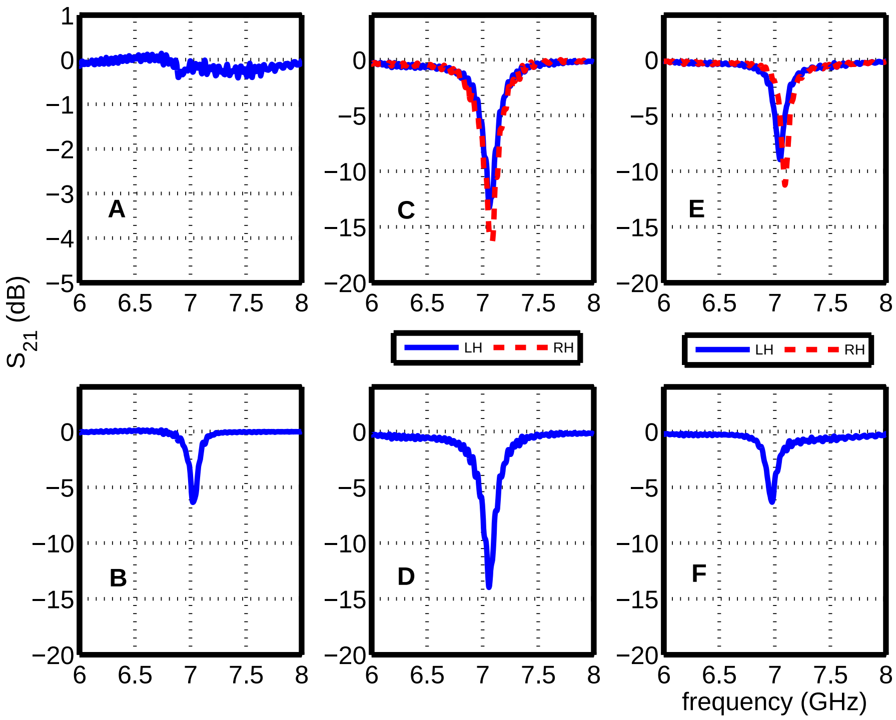

Figure 2.4: The experimental spectra of the canonical spiral with left helicity (solid blue) and right helicity (dashed red), corresponding to six orientations depicted in Fig. 2.1. A good agreement is present with the simulation results. Note that the resonance induced by magnetic coupling (E, F) are weaker in comparison to the electrically excited ones (C, D).

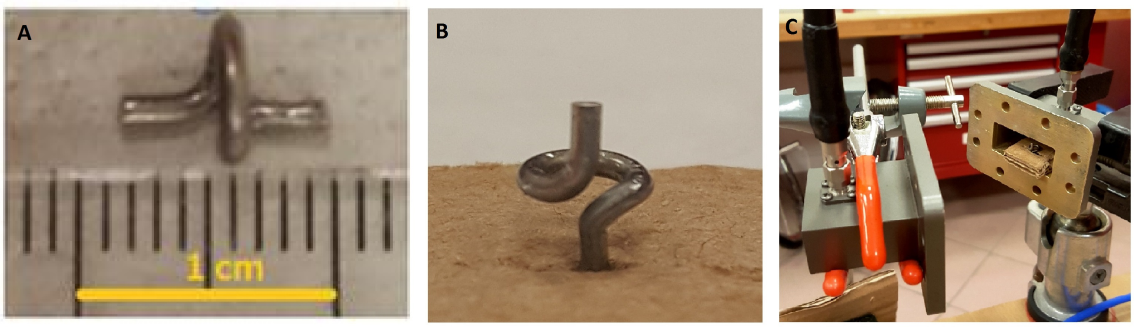

Figure 2.5: The canonical spiral sample (given a ruler in cm) used in measurements inside the waveguide.

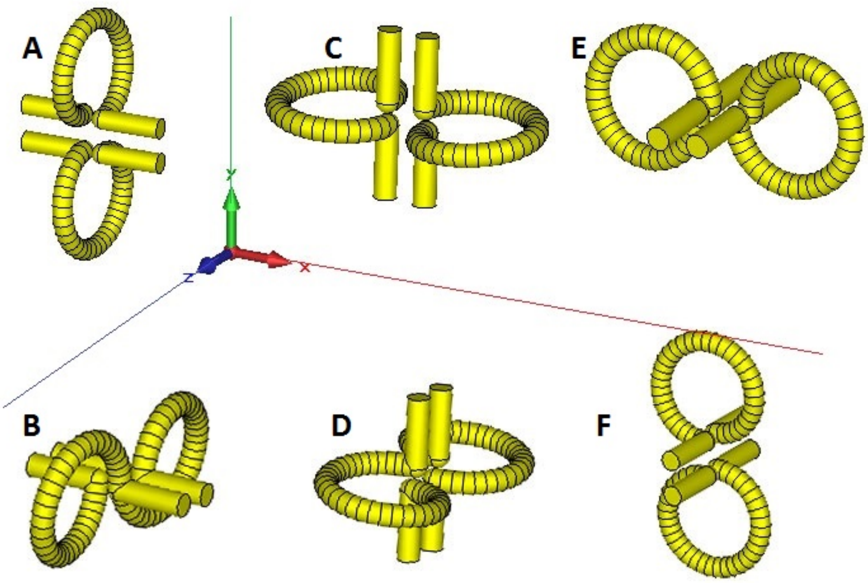

Figure 2.6: The possible configurations of the rod coupled spiral pairs are shown.A-B are the orientations where the rods are along the incident wavevector, k, and the gap is positioned a/symmetrically relative to electric field. In C and D, the staight wires of spirals are parallel to the incident polarization. C and D differs in the placement of the interspiral gap as parallel to the incident wavevector (C) and as parallel to incident magnetic field (D). In E and F, the spirals couple to the incident magnetic field. In E, the interspiral gap is parallel to the incident wavevector. In F, the interspiral gap is parallel to the incident polarization.

2.2 Coupled canonical spirals

2.2.1 Rod coupled canonical spirals

In this section, same handed and opposite handed canonical spirals are coupled to each other. Evidently, the spatial configuration between the spirals can be formed in an arbitrary way. Here, we limit our study to the coupling with the loop gaps facing each other and the straight wires of the spirals being parallel. This provides a strong coupling between the individual spirals. Henceforth, this coupling configuration will be called as "rod coupled canonical spiral pair". We investigate below the electromagnetic response of the rod-coupled canonical spiral pair following the same orientation convention given in Fig. 2.1.

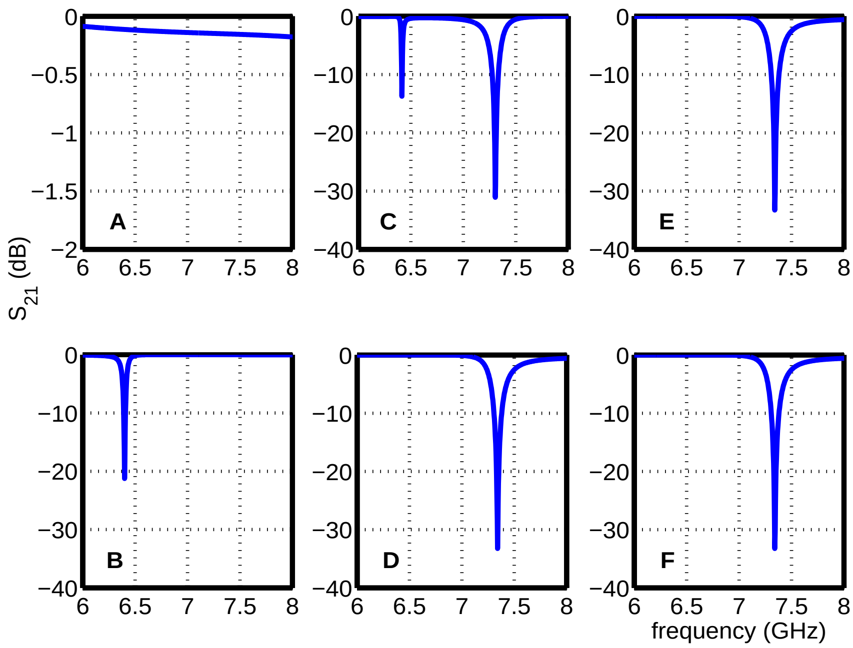

Figure 2.7: The simulated spectral response of the rod coupled same handed (either LH-LH or RH-RH) spiral pair are shown in six possible orientations.

For same handed (LH-LH) spiral pairs shown in Fig. 2.7.C, there is a resonance splitting depending on the coupling strength (i.e. coupling distance between the canonical spirals). Here, the interrod distance is taken as 1 mm. The resonance at lower frequency (6.4 GHz) is weaker than the resonance at the higher frequency (7.3 GHz). The current directions along the loops are opposite at lower resonance and same at higher resonance (Fig. 2.8). Similarly, the normal component of electric field plots can be used to define the symmetric and antisymmetric mode. The higher frequency resonance is associated with the symmetric mode where the same sign charges accumulate on the same sides of the gaps (the same ends of the straight wire segments) drived by the currents having same flow direction. The lower frequency is associated with the antisymmetric mode where the opposite sign charges accumulated on the neighboring sides of the gap (at the ends of the straight wire parts of the respective spirals).

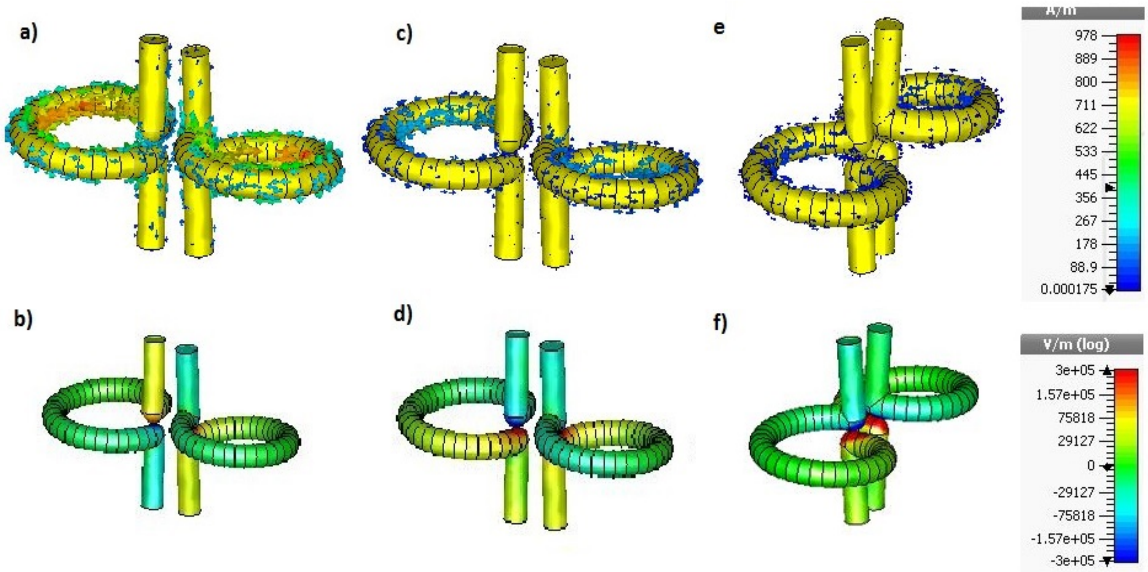

Figure 2.8: The current and normal electric field distributions are plotted at 6.4 GHz (a-b) and at 7.3 GHz (c-d) for the orientation C. (e-f) current and normal electric field distribution at the single resonance frequency 7.3 GHz of orientation D where the lower resonance cancelled.

In Fig. 2.7.D, we see that the antisymmetric resonance vanishes and only the symmetric mode resonance at the 7.3 GHz survives verified by the current distributions and normal E distributions (Fig. 2.8). To clarify, in these two electrically driven orientations the spirals are not excited magnetically. The resonance splitting occurs due to asymmetic positioning of the spiral pair with respect to propagation direction [47]. However if we separate the spirals, the splitting cancels out due to reduced coupling ending up single spiral resonance.

In the case of Fig. 2.6.A, since neither of the spirals couple to the incident wave, there is no resonant response in coupled configuration, either. Fig. 2.7.B shows a single electrically excited magnetic resonance that is shifted close to 6.5 GHz due to the coupling between the spirals and the current flow along the loops are in opposite directions(Fig. 2.9) leading to opposite sign charge accumulation at the edges of the interspiral gap. Thus, the total capacitance is enhanced and the resonance frequency is shifted to lower frequency.

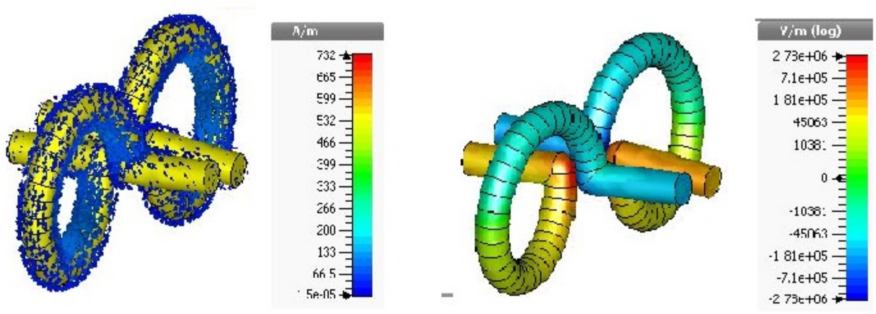

Figure 2.9: The current and normal electric field distributions are plotted at 6.5 GHz for orientation B. The oppositely directed currents result in a opposite sign charge accumulation at the edges of the gap. The sign of the charges can be interpreted as positive reading the electric field plotted as red and negative as blue.

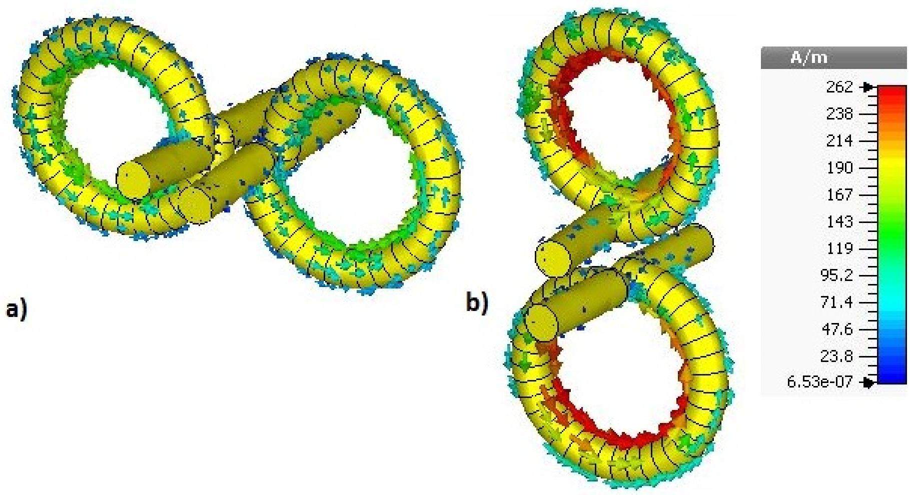

Figure 2.10: The current distributions are plotted at 7.3 GHz for orientations E-F where spirals are magnetically driven. In each case the currents along the loop flow in the same direction.

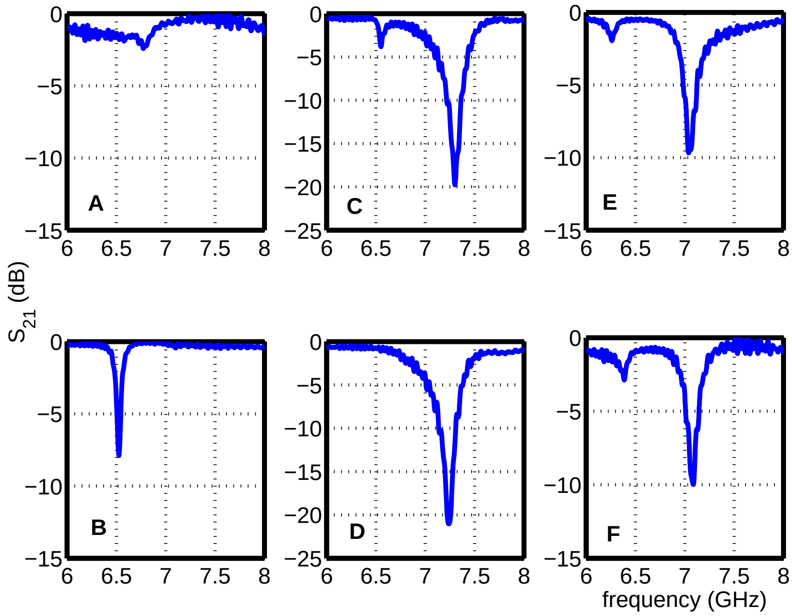

Figure 2.11: The measurements show similar features with the simulations. The nonresonant behaviour of the spiral in orientation A and the electrical excitation of the magnetic resonance is clearly observed. In electrically driven case, for the symmetric incidence (D) the surviving resonance is the higher frequency mode. The spectra for magnetically driven same handed rod coupled spiral pair show the stronger mode is at the higher frequency.

When the spiral pair is magnetically driven (orientations E-F), the spectrum exhibits only one dip for both a/symmetric orientation of intraspiral gap with respect to E field (Fig. 2.7) at 7.3 GHz. The currents along the loop flow in the same direction (Fig. 2.10).

We obtained the resonances for same handed rod coupled canonical spiral pair experimentally and the spectra for each orientation are plotted in Fig. 2.11.

For pair A, the measurement is in good agreement with the respective simulation. The small feature noticeable around 6.7 GHz is caused by alignment problems of the spirals within the pair as it does not show up consistently among different measurement batches. Despite the fabrication and alignment problems, measurements are matching quite well the simulated results in all cases. In the spectrum for B, the

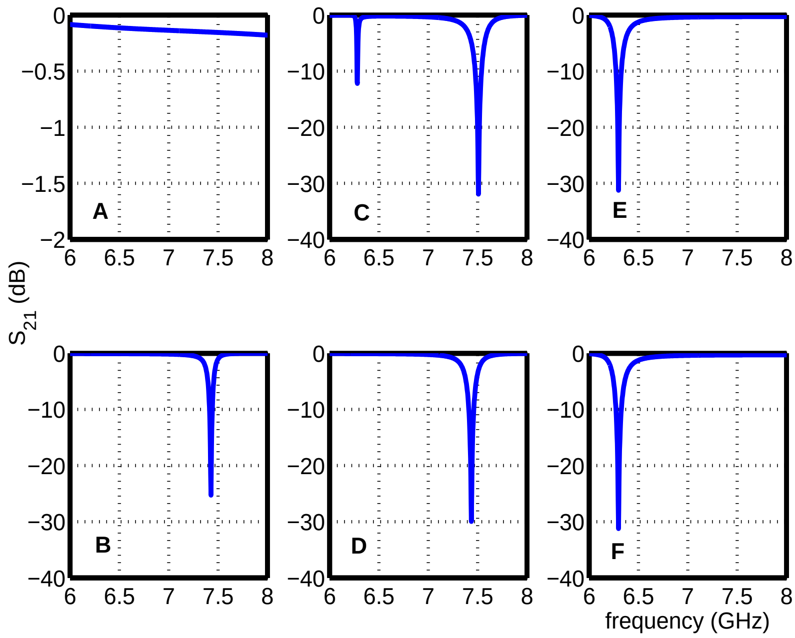

Figure 2.12: The simulated response of the rod coupled cross handed spiral pair are shown. (A) There is no any resonance following the single spirals behaviour.(B-F)various resonances are seen around 6.3 GHz and 7.5 GHz. (C) displays two resonances whereas D, the rotated case of C, posses only the higher resonance where the lower one is suppressed.

single resonance dip is at 6.5 GHz and it is weaker than the resonances for other orientations likewise to the simulated data plots. For C, the resonance splitting is observed at 6.5 GHz and 7.3 GHz, for D only resonance at 7.3 GHz survives. However, for E-F, there are two resonance dips, and here again, alignment problems cause the experimental resonances to deviate from the simulated ones by roughly 0.3 GHz.

For the pairs composed of cross handed spirals, the spectra for possible configurations are shown in fig. 2.12 and fig. 2.13 obtained from the simulated and measured data respectively. In contrary to the same handed pair spectra, in orientation B, the electrically excited magnetic resonance at higher frequency (7.5 GHz) is formed; for magnetically driven orientation (E-F), the resonance at lower frequency (6.3 GHz) is picked. We can explain the shift from single spiral resonance 7.04 GHz to rod

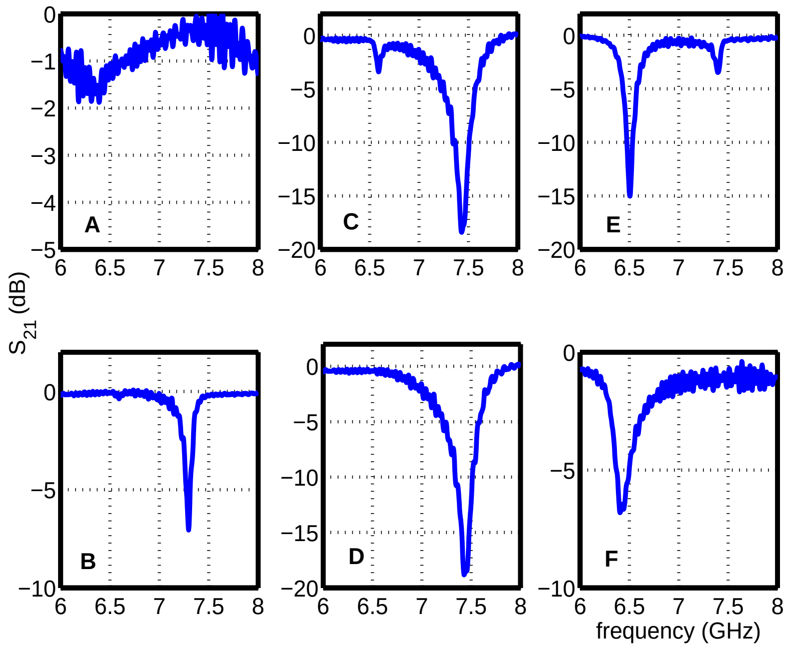

Figure 2.13: The cross handed rod coupled spiral pair spectral measurements are plotted for each orientation A-F.

coupled F configuration resonance 6.3 GHz based on the study in ref. [48]. This orientation is associated with negligible magnetic field between the canonical spirals but with strong electric field localization, indicating a capacitive coupling between the pair (fig. 2.14). The neighboring gaps of spirals lead to strong charge accumulation, so the coupling is mainly through the capacitance developed between the spirals in parallel with the individual rings capacitance. On the basis of LC circuit model of a split ring resonator, this additional capacitance results in the increase of the total capacitance of the system and thus to decrease of the resonance frequency. By using the same argument, the slight shift of the resonance of same handed rod coupled pair in the same orientation F can be explained by the interplay between inductive and capacitive coupling. In such case, still electric field is highly localized between the canonical spirals due to the gaps, however in detailed view, the magnetic field is more spread in the interspiral region for same handed pair in comparison to cross handed

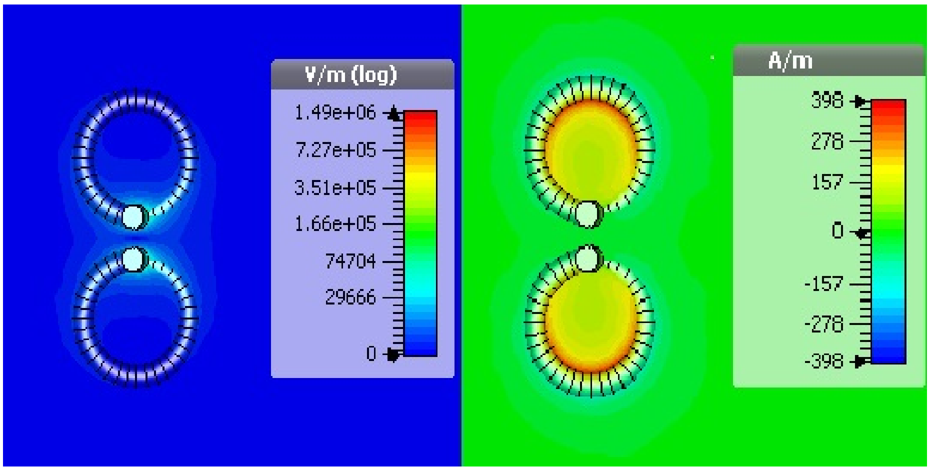

Figure 2.14: Electric field amplitude (a) and the magnetic field component Hz (b) at the resonance frequency is plotted for rod coupled cross handed spiral pair in orientation F. (a) Higher electric field intensity occurs in the gaps and in the region between the two spirals. (b) shows circular currents of the same direction in both rings and the negligible magnetic field in the region between the loops.

pair. The measurement supports the numerical results and even it demonstrates the slight difference in resonance around 7.5 GHz between B-C-D.

The effect of the chirality of the canonical spirals forming the rod coupled pairs can be summarized as follows: In orientation B, the magnetic resonance by electrical excitation occurs at lower frequency for same handed, at higher frequency for opposite handed pair. In electrically driven orientation symmetric and antisymmetric resonances are obtained, and the symmetric mode at higher frequency survives. The splitting is higher for cross handed pair. The current directions are reversed even they give the same spectra for cross handed pair. For magnetically driven resonators, the resonance shifted to higher frequency for same handed(inductive coupling), to lower frequency for cross handed pair(capacitive coupling) relative to single spiral resonance.

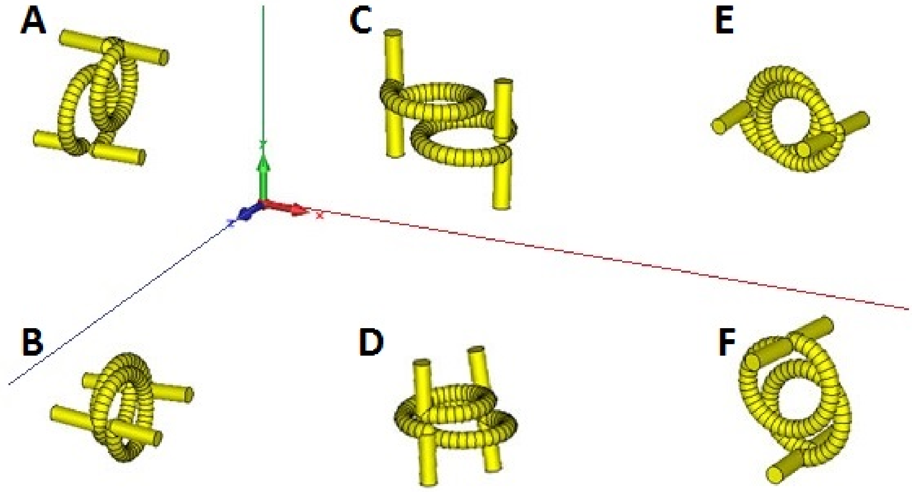

Figure 2.15: The orientations of the loop coupled spiral pairs are depicted. A-B rods parallel to the propagation direction (along x-axis), C-D rods parallel to the electric field (along y-axis), E-F rods parallel to the magnetic field (along z-axis).

2.2.2 Loop coupled canonical spirals

In this section, we study the loop coupled spiral pair that is formed by either same handed or opposite handed spirals bringing their loops on top of each other and leaving the straight wire segments at far sides (fig. 2.15). The distance between the loop planes are 1.4mm. The same orientation convention with single or rod coupled pair (A-F) follows also in this section.

Firstly, we study the pairs composed of same handed spirals. For the orientation A, there are two dips at 6.4 GHz and 8 GHz unlike the single spiral and rod coupled pair in the same orientation where a resonance was not observed due to symmetric positioning of the gap diameter with respect to electric field and it was not magnetically excited. If the facing loops of the each spiral lie on the same yz plane, the simulations show that the resonance disappears. In order to superpose them, the loop planes are shifted. So, this coupling leads to two weak resonances. In B, a single resonance dip at 8 GHz is seen. In the measurements, the dip at lower frequency is much weaker but still detectable. In Fig. 2.16.C the resonance at 6.5 GHz is stronger than the resonance

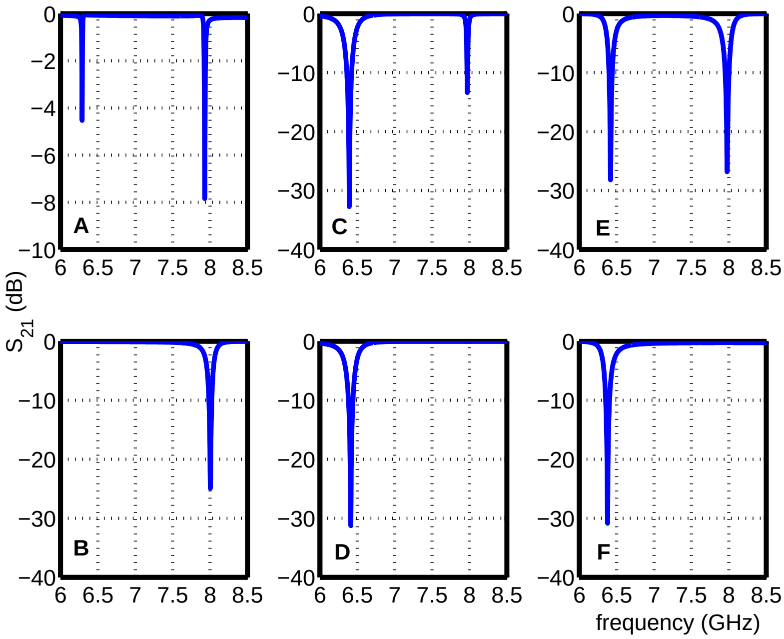

Figure 2.16: The loop coupled same handed spiral pairs spectral response are computed for each orientatin A-F. The strong coupling results in higher splitting with respect to rod coupled case. The two resonances are at 6.5 GHz and 8 GHz.

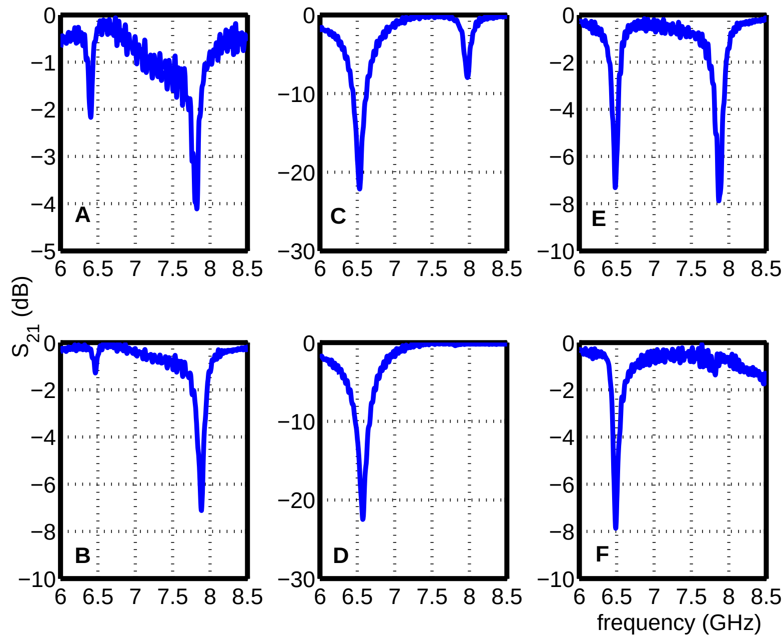

Figure 2.17: Experiments show that the same handed loop coupled spirals posses two resonances at 6.5 GHz and 8 GHz at the selected coupling distance verifying the spectral simulation results.

at 8 GHz satisfied also by measurements. In Fig. 2.16.D the resonance at lower frequency is survived whereas in rod coupled pairs the resonance at higher frequency was survived (fig. 2.7.D). The current directions around the loop are the same. For the lost resonance, we see that the current directions are opposite cancelling out the net magnetic dipole in this symmetric orientation with respect to the incidence of the excitation. For the orientation E, there are equally dominant resonance dips in the spectrum which are at 6.5 GHz and 8 GHz. At lower frequency the current directions are the same and the resonance is associated with the magnetic resonance due to magnetic-electric excitation. At higher frequency, the electrically excited resonance is observed since the current flows around the loop in opposite direction so that the magnetic dipoles cancel out. In F, only the magnetic resonance survives supported by the same flow direction of the currents producing net magnetic dipole. Since the spirals symmetry axis sees the electric field, the electrically excited resonance at higher frequency is destroyed. The current directions at that lost resonance frequency are opposite and much smaller in magnitude compared to the results for E. The measurements are matching the simulated spectra (Fig. 2.17).

Secondly, cross handed loop coupled spiral pair is investigated. Their simulated and measured spectra are plotted in Fig. 2.18, 2.19, respectively. A,B,E,F show similar patterns with the same handed loop coupled pair spectrums. However, for cross handed loop coupled pair in C,D orientations, the resonance at higher frequency (8 GHz) is stronger and the surviving resonance dip is at that frequency while changing the orientation from C to D. The weaker resonance is at 6.4 GHz. The measured spectral data matches the numerical results for first four orietations, but in Fig. 2.19.E,F the spectra are shifted to the lower frequencies. In orientation C, the current directions around the loop are the same at lower frequency, and opposite at higher frequency. The resonance dips magnitude reversed due to helicity reversal. Since the opposite current directions in opposite helicity spirals produce the net magnetic dipole in the same direction in contrast to the same handed loop coupled pair resonances having the oppositely directed current flow. The magnitude of the current

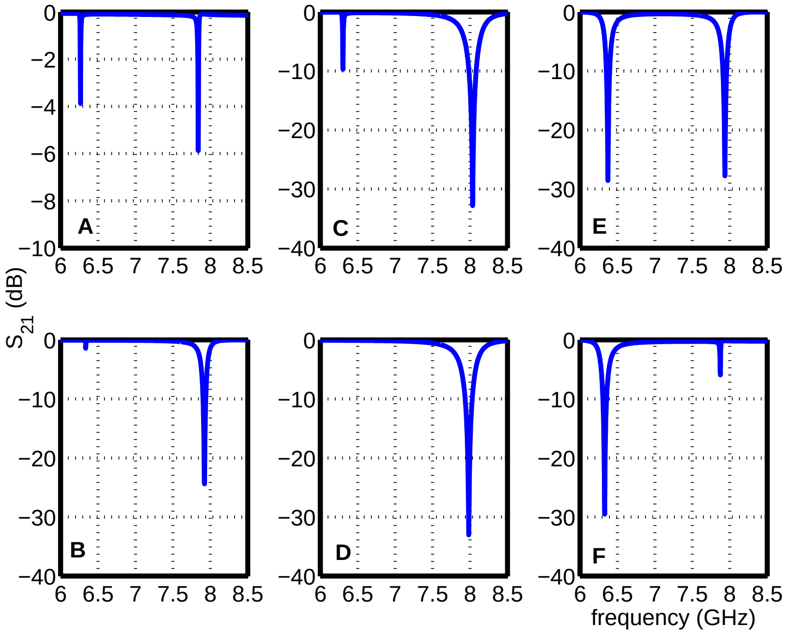

Figure 2.18: Spectral simulation results of the loop coupled opposite handed spiral pair are plotted. The two resonances are located close to 6.4 GHz and 8 GHz.

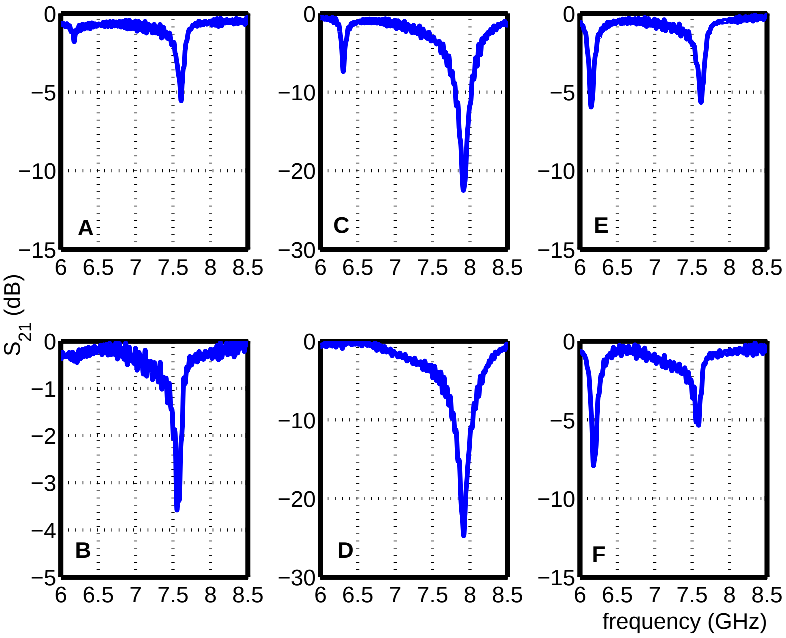

Figure 2.19: Loop coupled opposite handed spiral pair examined experimentally where the similar patterns and resonances are observed with the simulated spectra.

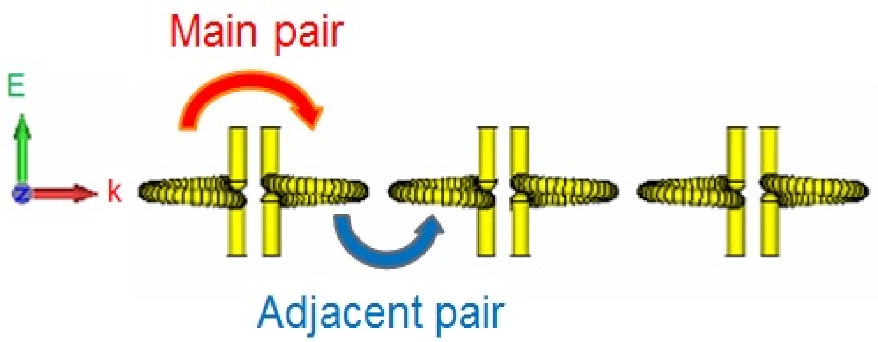

Figure 2.20: The main and the adjacent pairs forming the chain of three rod coupled canonical spiral pairs are shown. The rods are eletrically driven and the chain is positioned along the propagation direction.

at the dominant resonance is lower compared to current magnitude at the weaker resonance. This observation is valid for both same and cross handed spiral pair. In orientation E, independent of the helicity of the pair the same spectra are obtained with two resonances with same magnitude.

As a conclusion, independent of chirality, at low frequency mode, the current directions along the respective loop parts of the spirals are always same, at higher frequency the current flow is opposite. In cross(same) handed , opposite (same) currents produce net magnetic dipole. So, for same handed pair, low frequency mode is stronger and the surviving one in the symmetic wave incidence orientation (electrical excitation of the magnetic resonance). In contrary, for cross handed pair, high frequency mode survives.

2.2.3 Chain of coupled canonical spirals

This section investigates the linear chain of rod coupled canonical spiral pairs that are positioned along the propagation direction and the wire segments are parallel to the incident polarization. We approximate a long chain by using nine pair elements in the simulations. Limitations of the experimental setup restricted the chain to consists of at most three coupled pairs. Thus we simulated the three coupled chain for comparison as well. In Fig. 2.21, both the experimental and numerical results are shown for 1, 2 and 3 pairs of rod-coupled spirals. We observe that increasing the number of pairs in the chain widens the resonance dip of a single rod-coupled spiral pair, thereby generating a stop band. The comparison of experimental and simulation results show certain discrepancies. The measured stop band is wider in the experiment. This is dominantly caused by the uniformity problems of the fabricated spirals and their positioning within the chain. Deviations from structural parameters for the individual spirals and the chain cause a spectral broadening. Nevertheless, the number of humps within the gap are consistent with the number of resonators pairs in the chain both in simulations and experiment.

The electromagnetic response of a long-chain consisting of nine rod-coupled spiral pairs is studied under 4 configurations: same handed pair and same handed adjacent (Fig. 2.20) (i.e.,(LH-LH)+(LH-LH)), same handed pair and opposite handed adjacent (i.e., (LH-LH)+(RH-RH)), opposite handed pair and same handed adjacent (i.e.,(LH-RH)+(RH-LH)), opposite handed pair and opposite handed adjacent (i.e., (LH-RH)+(LH-RH)). Figure 2.22 shows the simulated transmission spectra of each configuration (blue curves). For comparison, the resonance spectrum of a single pair for each case is also plotted (red curves). We observe that each configuration opens stop bands around the resonance modes of the single pair within the chain. When the helicity of the spirals in adjacent pairs is the same (Fig. 2.22.a-b) the stop band at the high frequency mode is enhanced both in terms of bandwidth and s/n ratio. When the adjacent pairs have opposite helicity spirals in neighbor (Fig. 2.22.c-d), the stop band around the low frequency mode of the single spiral is broadened, although the enhancement is lower than that of the former case. The adjacent pairs with neighboring spirals of opposite helicity favor the magnetic resonance mode of a rod-coupled spiral pair. The mechanism is related to the loop-coupling between adjacent pairs, where the current flow in the same or opposite directions enhances either of the resonance modes of the single pair.

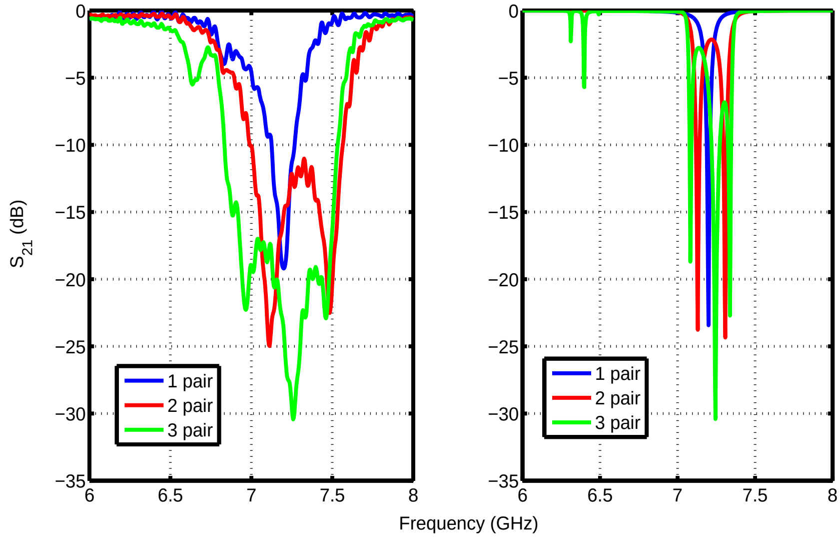

Figure 2.21: The measured (left panel) and simulated (right panel) data is plotted for single(blue) , double (red) and chain of three (green) same handed pairs.

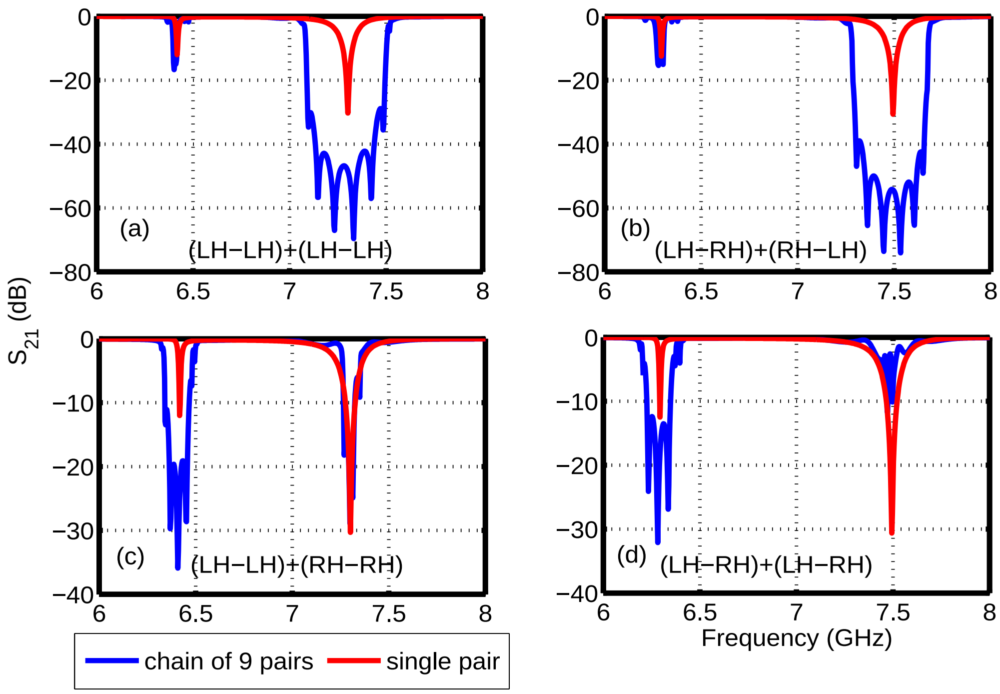

Figure 2.22: The spectra for chain of 9 pairs are plotted (a) same handed main, same handed adjacent (b) cross handed pair, same handed adjacent (c) same hande pair, cross handed adjacent (d) cross handed pair, cross handed adjacent. The single same handed rod coupled pair resonanances are at 6.4 GHz and 7.3 GHz, the single opposite handed rod coupled pair resonances are at 6.3 GHz and 7.5 GHz.

Chapter 3

OPTICAL FORCES ON CANONICAL SPIRALS

3.0.4 Single canonical spirals in optical regime

For a metallic nanoparticle the optical force can be enhanced significantly, if the light can also excite the plasmonic resonance of the nanoparticle and hence generate strong localized electromagnetic fields. For typical inert metals (e.g., gold, silver) and nanoparticle sizes (approximately 100 nm) this is achievable at visible and near infrared wavelengths. The presence of chirality in the plasmonic nanoparticle enriches the optical forces further, by generating an angular momentum in the local fields. In turn, this force can be utilized to manipulate chiral particles optomechanically. With this motivation, the present section employs canonical spiral design for plasmonic chiral nanoparticles and investigate the optical forces on the canonical spiral nanoparticles in single and coupled configurations. The canonical spiral consists of a loop of radius $r = 50$ nm and the pitch $p = 50$ nm, two wires attached to the ends of the loop of length $l = 100$ nm and the minor radius is $r_0 = 12.5$ nm depicted in fig. 3.1. The canonical spirals in orientations A-F (Fig. 3.2) are under the linearly polarized plane wave incidence where the electric field is along the z-axis and the propagation along x-axis. The optical forces are calculated by taking the surface integral of the Maxwell Stress Tensor on a closed capsule of similar shape with the gold canonical spiral. The numerical computations are held in Comsol software [49] . Although the magnitude of the forces seem to be very small, they are compatible with the piconewton forces shown in a recent study [45] after the necessary conversion of the incident power density.

The x-,y-,z- components of the optical force for each orientation is plotted in Fig. 3.3. A, F posses two peaks at 680 nm and 1125 nm. The rest exhibits resonances

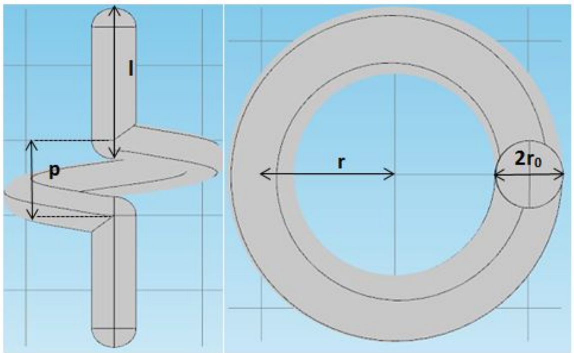

Figure 3.1: The geometrical parameters of a single canonical spiral are shown. The loop radius $r = 50$ nm, the diameter of the rods $2r_0 = 25$ nm, length of the rods $l = 100$ nm and the pitch $p = 50$ nm.

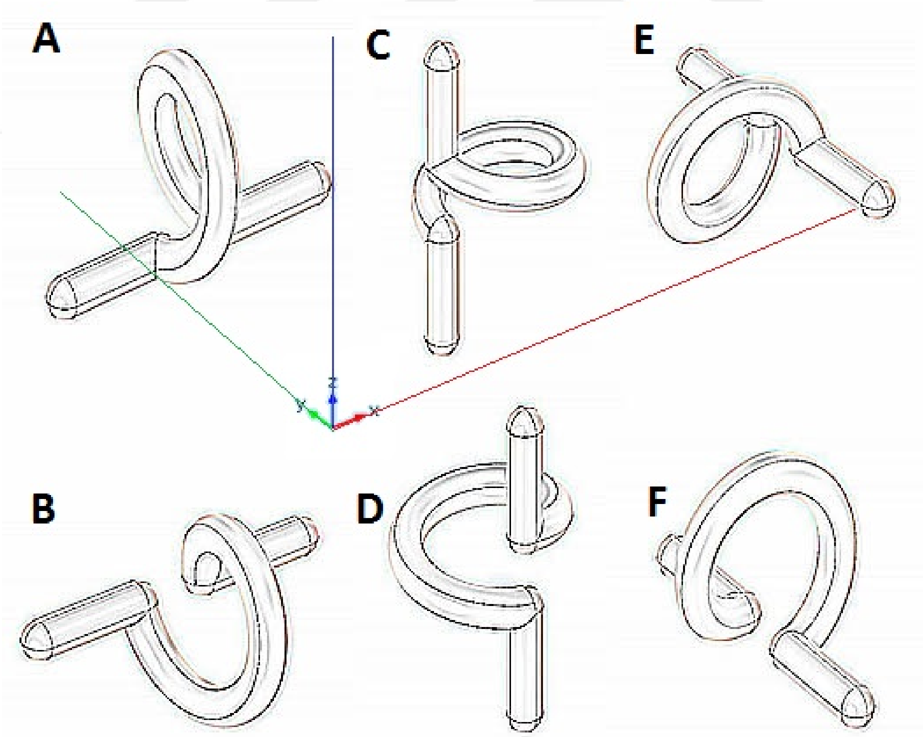

Figure 3.2: The orientations A-F of the canonical spiral in given coordinate system is shown. (A-B) the rods are along the propagation direction, (C-D) the rods are along the electric field, (E-F) the magnetic field passes through the loop.

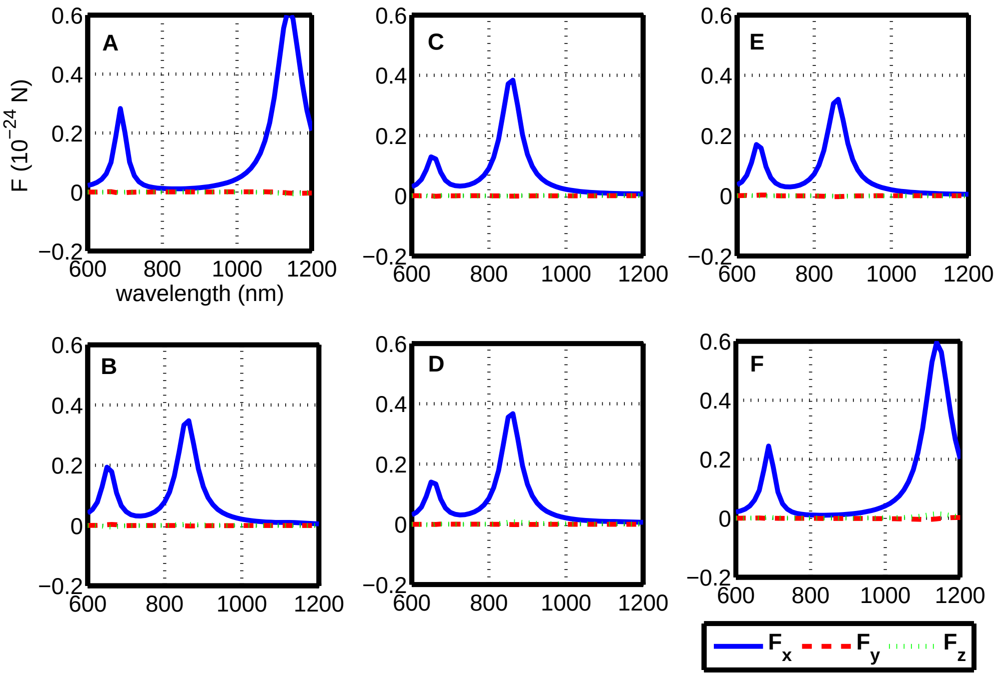

Figure 3.3: f_x (blue solid), f_y (red dashed), f_z (green dotted) spectra are plotted for orientations A-F. The scattering force f_x shows two peaks at 680 nm and 1125 nm for A-F, at 650 nm and 860 nm for B-C-D-E. The other force components f_y and f_z are negligibly small.

at 650 nm and 860 nm nearly at same magnitudes. The spiral experiences only the scattering force, f_x, that pushes along the propagation direction. The lateral force, f_y, and the f_z are negligibly small as expected.

If we compare the optical force components calculated for wavelengths between 600 nm-1300 nm of two orientations A-B, it seems that the resonant peak at longer wavelength (1125 nm) is shifted to a lower one (860 nm). However, the orientations between these two corresponding 0° and 90° by taking the angular steps by 30°, we see that one more resonant peak is formed and intensified, then the peak at longest wavelength is suppressed as shown in Fig. 3.4.

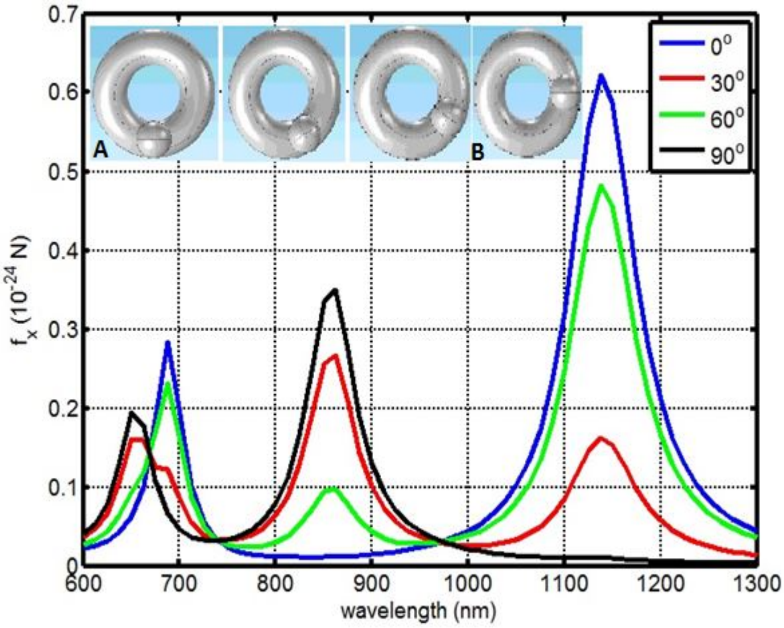

Figure 3.4: f_x is plotted for orientations starting from A ending in B by taking 30° and 60° rotations. $f_{y,z}$ are not plotted because of negligibly small magnitudes. The orientations corresponding to 0°, 30°, 60° and 90° are shown inset from left to right in order.

In summary, the single canonical spiral in the visible range posses two resonances for all six possible orientation and they reveal in the calculated x-component of the optical force haiving two maxima at the resonance wavelengths. The other force components are significantly small to be neglected.

3.0.5 Rod coupled canonical spirals in optical regime

In this section, we analyze the response of the rod coupled canonical spirals by restricting the wavelength range between 600 nm-800 nm. The rod segments are parallel to each other and the gaps are at the closest position. The rod coupled pairs can be classified as same handed or opposite handed that takes six possible orientations.

Firstly, for same handed rod canonical spirals in Fig. 3.6.A, f_x, positive scattering force along the propagation direction is still observed equal as expected for each spiral(1,2). The lateral force, f_y, is negligibly small, and f_{1z}, f_{2z} are in opposite

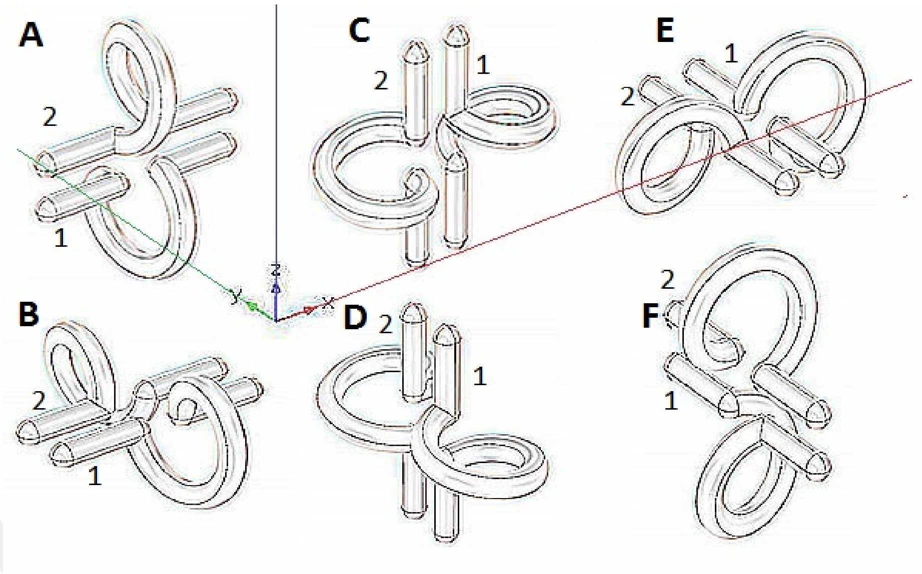

Figure 3.5: The orientations named from A to F of the canonical spiral in given coordinate system is shown.

direction and of same magnitude. We define the relative force as $f_{rel} = (f_1 - f_2)/2$ to describe the optical force between the spirals and the common force as $f_{com} = (f_1 + f_2)$ which is the force acting on the center of mass of the spiral pair. From the sign of the forces, we deduce that the z-component of the relative force f_{rel_z} is positive along the z-axis, so the f_{rel_z} is attractive and the spirals tend to approach each other. The f_{com_z} is zero, so the center of mass of the spiral pair would not move along the z-axis (Fig. 3.7.A). For orientation B, which is the case when A is rotated 90 degree about x, f_z becomes zero, f_x , the force that pushes the spirals, survives, f_y are formed which are same in magnitude, but opposite in sign. Thus, f_{rel_y} is attractive (Fig. 3.7.B). The same obtainings are valid for F. In the case D, the neighboring spirals are in y -direction leading to repulsive f_{rel_y} in contrast to B although the forces are weaker. In C, spirals are aligned along the propagation direction and the electric field is along the wires. The force components other than the f_x are zero. Force on latter spiral f_{1x} is all positive whereas the former one, f_{2x}, changes sign from positive to negative. The results for E carry similar features with C, but the behaviour of f_{1x} and f_{2x} is reversed.

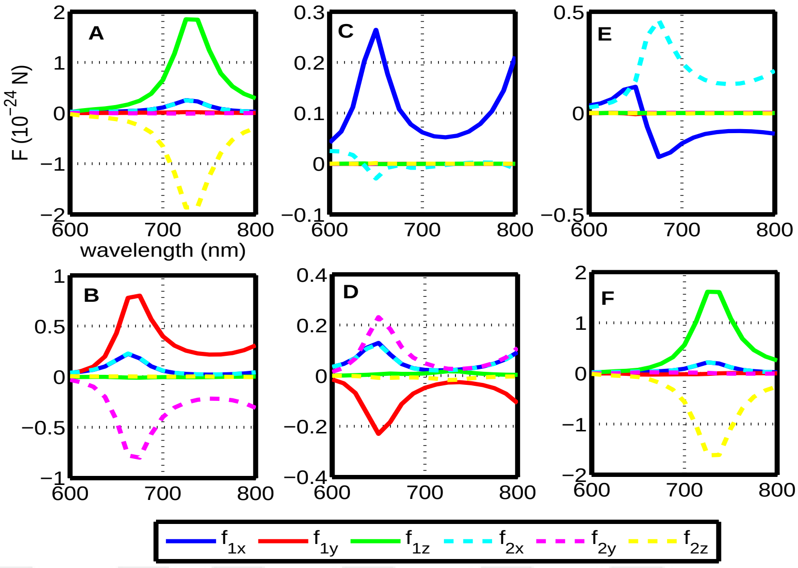

Figure 3.6: The optical force components $f_{1_x}, f_{1_y}, f_{1z}, f_{2_x}, f_{2_y}, f_{2_z}$ spectra for the rod coupled canonical spiral pairs having the same handedness are plotted for each orientation A-F. If the coupled geometry is aligned on z-direction, f_z is formed(A,F). f_y is revealed when the pair is coupled along y-axis (B,D). Asymmetric response in f_x is observed when the spirals are along the propagation direction(C,E).

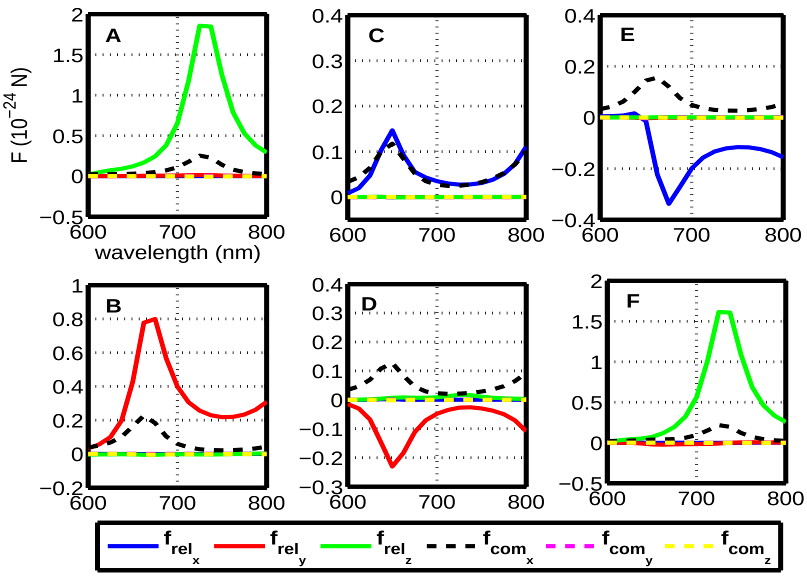

Figure 3.7: The relative and common optical force spectra for the rod coupled canonical spiral pairs having the same handedness are plotted for each orientation A-F. f_{com_x} is all positive verifying the scattering force exerted on the pair along the propagation direction and $f_{com_{y,z}}$ are zero. A-F exhibit relative attactive force in z direction, B shows that spirals repel each other in y direction whereas f_{rel_y} is attractive for D. The f_{rel_x} is repulsive in C, in contrary to E.

We can conclude that the rod coupled pair as a unique object does not feel any force in y- and z- direction as f_{com_y}, f_{com_z} are zero in all orientations, and it experiences a pushing force along the plane wave propagation direction. However, the pair components can apply forces on each other either repulsive or attractive force relatively in all three directions depending on the orientation. This forces may result from the chiral fields produced by individual spirals and the coupling of these near fields lead to either attractive or repulsive forces between them. The magneto-electric coupling between the electric and magnetic dipoles shows itself as a chiral part of the optical forces studied in [43, 51]. The chiral and achiral optical force expressions are given in appendix taken from ref.[43].

Secondly, we study the optical forces on the cross handed rod coupled spirals. Fig. 3.8.A-F shows that $f_{rel_{x,y}}$ are zero. The resonance is at 725 nm at which gives f_{rel_z} maximum. The coupling along z direction leads to the formation of f_z of same magnitude but opposite in sign, so f_{rel_z} is attractive but in total f_{com_z} is zero. The pair is not affected by $f_{com_{y,z}}$. f_{com_x} is weaker than the f_{rel_z} that continues to push the pair along the propagation of the wave. In Fig. 3.8.B-D, a repulsive relative lateral force f_{rel_y} is seen and f_{com_x} is positive giving the expected result. Other common and relative force components are zero. Fig. 3.8.C, the spirals relatively repel each other in the propagation direction, we read f_{rel_x} is repulsive. In E, fy, fz are calculated as zero, only f_x along propagation diretion is noted around 660 nm resulting in an attractive f_{rel_x}.

The comparison between same and opposite handed spirals demonstrates that the results for A are not affected by the change of handedness. The relative lateral force reversed from attractive for same handed pair to repulsive for opposite handed pair in orientation B. As it can be seen in the Fig. 3.9, for same handed pair, the electric field x-component distributions lead to the opposite sign charges accumulation at the edges of the adjacent spiral legs and the interspiral gap. However, for the opposite handed pair, the charges at the edges of the adjacent spirals are of the same sign. Handedness does not change the force results in D; in case of E the positive region of

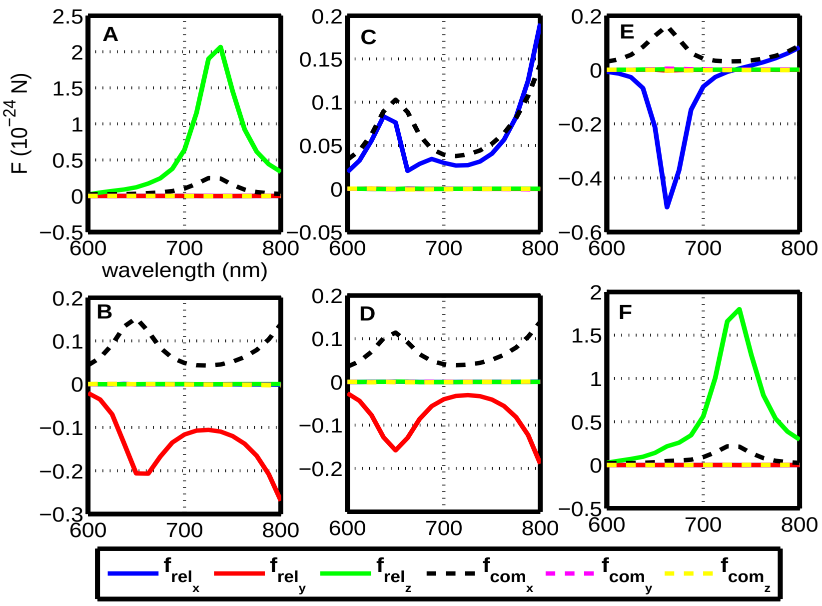

Figure 3.8: The spectra of the components of f_{rel} and f_{com} of the cross handed rod coupled canonical spirals in orientations A-F are plotted. The common forces in y,z are not detected. The scattering force acting on the c.m. of the pair is still in +x-direction. A,F show attractive relative force in z; B,D show repulsive force on each other in y, C exhibits repulsive f_x whereas relative force in x for E is attractive

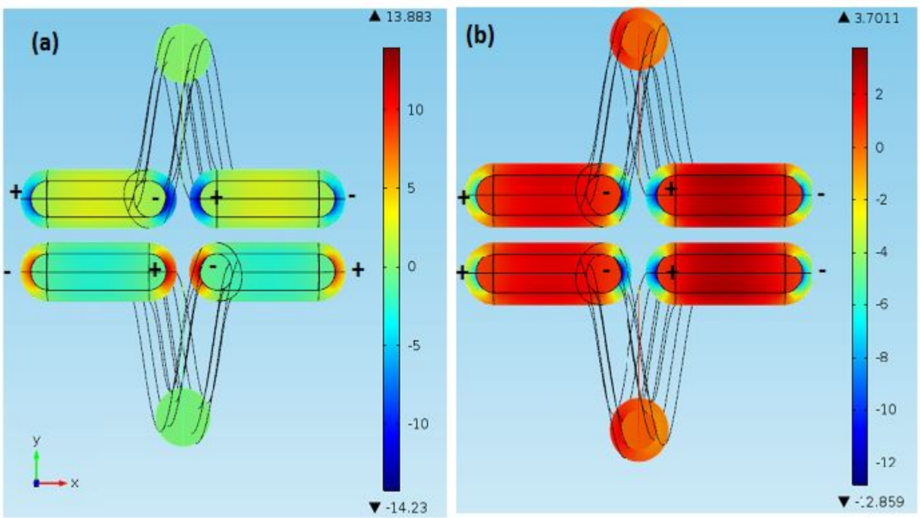

Figure 3.9: x-component of the electric field is plotted for (a) same handed and (b) opposite handed rod coupled pair in configuration B. The sign of the charges at the edges are shown that results in (a) attractive or (b) repulsive relative force in y-direction.

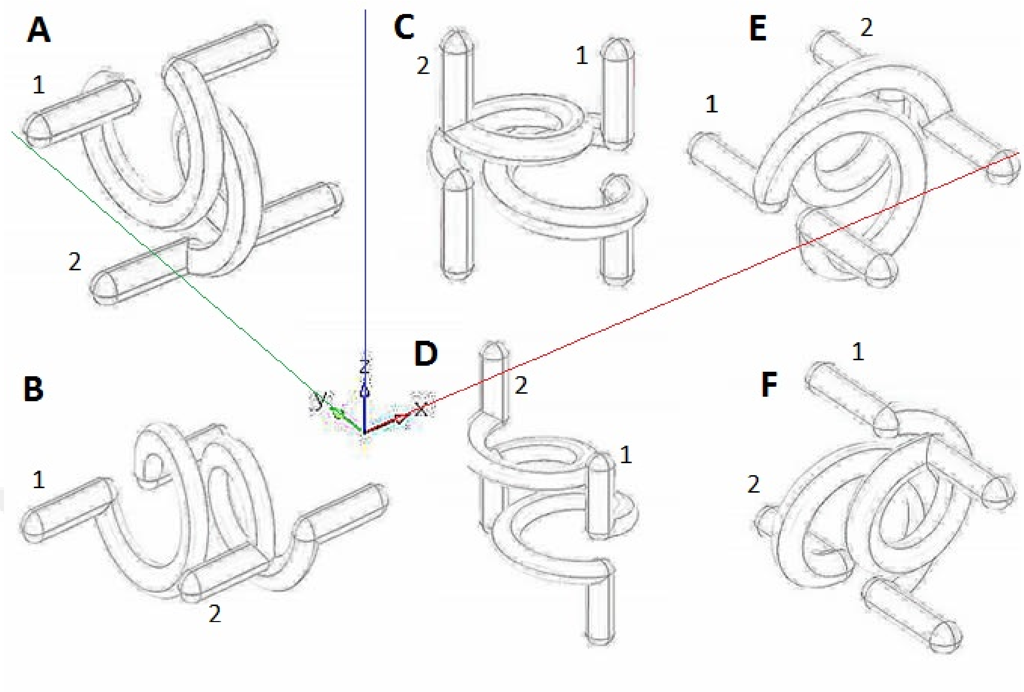

Figure 3.10: The orientations named from A to F of the loop coupled canonical spirals in given coordinate system is shown.

f_1x for same handed pair is suppressed. Lastly, for F it is not seen any effect of the reversing the handedness of one spiral constituting the pair.

3.0.6 Loop coupled canonical spirals in optical regime

In this section, we investigate the loop coupled canonical spirals depending on the helicity of the spirals making up the pair. The loops are placed on top of each other, leaving the rod sections at far sides. Following the same naming of the possible orientations, the schematic are shown in Fig. 3.10.

For the same handed loop coupled pair, Fig. 3.11.A shows that f_{rel_z} changes from repulsive to attractive after a saddle point around 690 nm. Although the distinguishability is difficult for f_y for each spiral, it results in a repulsive f_{rel_y}. In Fig. 3.11.B, the resonance peak shifted to a lower wavelength of 640 nm. f_{rel_x} is repulsive for both A and B. In C, there exists a small relative repulsive f_y. The attractivef_{rel_z} is stronger than other force components. In D, the symmetric incidence of the plane

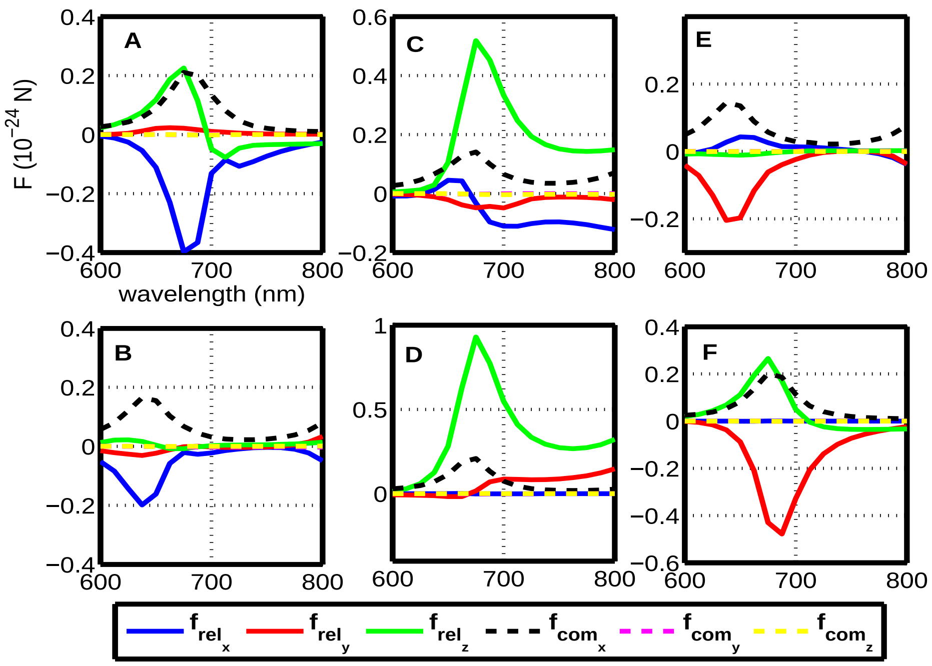

Figure 3.11: f_{rel} and f_{com} spectra of the same handed loop coupled canonical spirals in orientations A-F are plotted.

wave results in same $f_{x1,2}$ such that f_{rel_x} become zero. f_{rel_z} is attractive showing a peak at 675 nm. f_{rel_y} becomes attractive after the resonance wavelength. In E, the dominant force component is f_y leading to attractive relative f_{rel_y}. The spirals attract each other in x-direction. In F, f_{rel_y} is repulsive, and the peak is shifted to longer wavelength of 680 nm, f_{rel_z} is lower in magnitude with respect to attractive f_{rel_y}.

To summarize, the scattering force (f_{com_x}) is acting on the center of mass of the loop coupled pair in all cases. There is no net force acting on lateral and vertical directions. However, due to coupling between the spirals, relative repulsive or attractive forces with respect to the coupling directions are formed.

Secondly, the relative and common optical forces on the loop coupled pair consisting of opposite handed canonical spiral are analyzed.

The force components for each spiral are plotted separately in Fig. E.3. Based on the individual force components the relative and common forces are shown in Fig. 3.12. We read that for A f_{rel_x} is repulsive showing a peak at 675 nm, f_{rel_z} changes sign

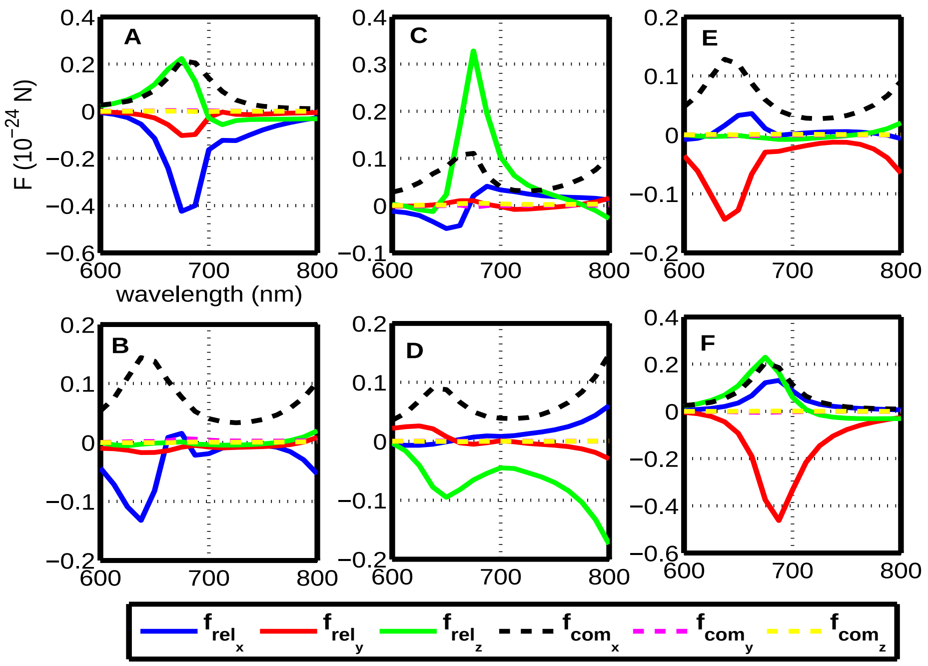

Figure 3.12: f_{rel} and f_{com} components spectra of the opposite handed loop coupled canonical spirals in orientations A-F are plotted.

so that it becomes attractive from repulsive. The similar behaviour is observed for lateral force in a reversed manner. For C, f_{rel_z} is attractive having the maximum at 675 nm. Since f_y on each spiral are very small, f_{rel_y} are not easily noticeable.f_{rel_z} becomes repulsive for D and it exhibits an attractive f_{rel_y}, but f_{rel_y} changes sign after 660 nm. In E, there is a significant repulsive force f_{rel_y} and the attractive f_{rel_x} which exhibits a peak at 650 nm. For F, $f_{rel_{y,z}}$ are both repulsive. The peak is shifted to a longer wavelength of 680 nm by going from E to F. In all cases, f_{com_y} and f_{com_z} is zero, and the usual radiation force is observed in f_{com_x} .

For the loop coupled spiral pair, the effect of changing the helicity of one of the spirals is summarized as follows: For the orientation A, the change in sign and magnitude of relative f_y (from repulsive to attractive force) is observed. For C, the force magnitudes are diminished and f_{rel_y} is all negative for same handed pair. In cross handed spiral case, although f_{rel_y} is very small in detailed view it changes sign. f_{rel_x} is reversed from negative to positive for cross handed pair and from positive to

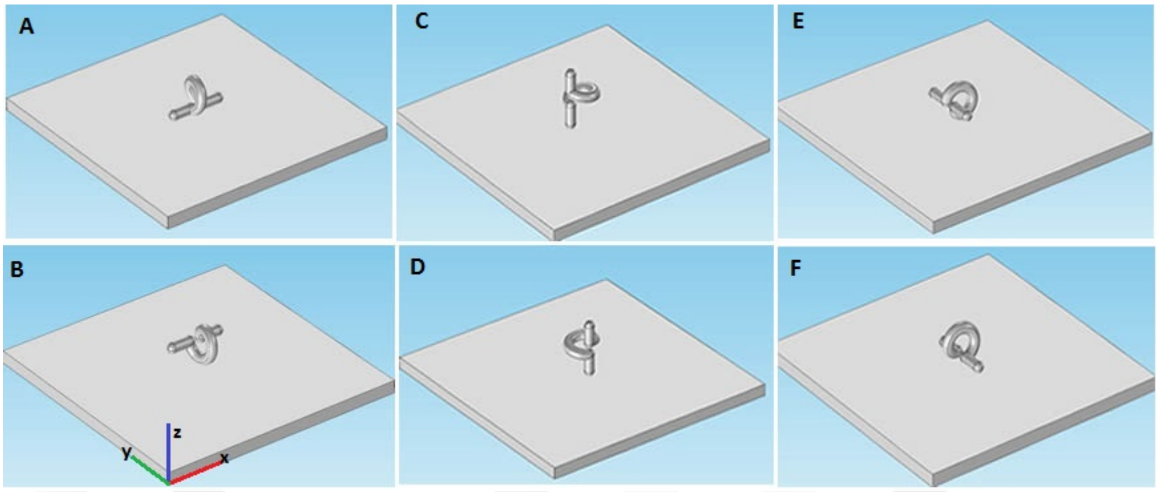

Figure 3.13: Single spiral placed above a gold sheet in 6 different orientations. Incident plane wave propagates along x-axis, and the electric field polarized along z-axis.

negative for same handed pair. In D, f_{rel_z} is reversed from attractive to repulsive. However in E, the relative and common force components does not change due to the reversal of the helicity. Lastly, in F, f_{rel_x} becomes repulsive where f_{rel_x} is zero for same handed spiral couple.

3.0.7 Single canonical spiral on a gold substrate

We have placed the single gold canonical spiral above to a gold thin sheet of dimensions 1 μm x 1 μm and of thickness 50 nm. The substrate lays on the xy plane (fig. 3.13). The presence of the substrate enhances the confined field in the region between the spiral and the gold layer which leads to an attractive force in the z direction. Also, the resonant peaks in force shifts to longer wavelengths compared to the single spiral optical force calculations as plotted in fig. 3.14.A,B,E,F. But they still preserve the other resonance which leads to stronger forces on the spiral. C,D orientations are actually the least coupled case, so we are still examining the not shifted first resonance wavelength of the single spiral, besides the formed attractive f_z. Also for these two orientations, the optical force components are relatively smaller than the others. The scattering force, f_x is always positive, but the magnitude changes, where the strongest

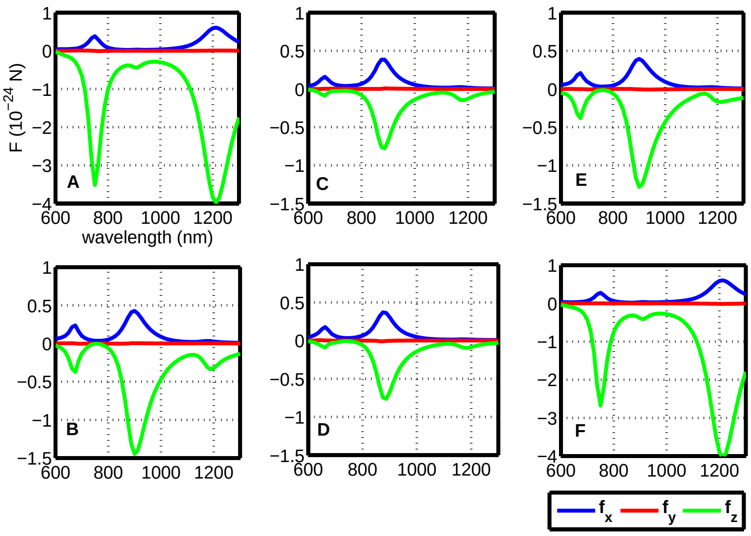

Figure 3.14: f_x(blue), f_y(red), f_z(green) exerted on a single canonical spiral above the gold substrate are plotted for wavelengths between 600 nm-1300 nm. f_y is negligible small for all orientations. The scattering force and f_z, which is towards the substrate, exhibits peaks at the resonant wavelength, which are at 660 nm, 675 nm and 750 nm, depending on the orientation of the spiral above the substrate. The second peaks in force plots are positioned at 880 nm, 900 nm and 1200 nm.

f_x are observed for orientations A and F. By rotating the spiral in A 90° about x-axis, we obtain the orientation B and we see that the peak is at 675 nm wheras for A it is at 750 nm. In all orientations we do not see any lateral force f_y. Contrary to our results, in study of Wang and Chan[45], the similar chiral object experiences a lateral force due to the presence of metal or dielectric substrate. The explanation comes from the coupling of the structural chirality to the fied reflected from the surface. At some point, we justify the same observations where increasing the number of turns of the spiral enhances the lateral force. The comparison between single and multiple turn spirals showed that we have got not zero f_y.

3.0.8 Rod coupled canonical spiral on a gold substrate

In this section, we investigate the effect of the gold substrate in the vicinity of the rod coupled spiral pairs. We have selected two orientations such that the coupling to the substrate is highest and both of the spirals are under this consideration, and also the spirals coupling scheme obeys our descriptions in the previous sections. Once again, the effect of the change of the helicity will be discussed. We have also restricted the range of wavelengths between 600 nm - 800 nm, but we noted that at longer wavelengths the second resonant behaviour survives even for coupled spirals like single spiral in free space or in the vicinity of the substrate.

First of all, we can say that since they are placed above the substrate f_z is formed for both same and cross handed case in contrast to free standing rod coupled spirals in the same configurations. When the spiral rods are along the propagation direction and the loops are looking towards y-axis, the lateral force between the spirals is attractive where two peaks are started to form in comparison to free standing rod coupled spirals (fig. 3.15.a). f_{rel_y} changes sign by taking opposite handed spiral pair (fig. 3.15.c). f_{com_y} is zero, f_{com_x} pushes the pair along positive x-axis and f_{com_z} is attractive towards the substrate.

In other orientation, relative and common forces are plotted in fig. 3.15.b,d for same handed and opposite handed pairs respectively. f_y is relatively small compared to the other force components. Similar to fig. 3.15.a,c the pair as a unique object experiences the repulsive common force in +x direction and the pair is attracted towards the substrate by f_{com_z}. f_{rel_x} changes sign for same handed pair whereas the cross handed spirals always attract each other. In contrast to f_{rel_x}, f_{rel_z} is all negative between same handed spirals, but it is changing from repulsive to attractive between cross handed spirals. There is no lateral force exerted on the center of mass of the pair. However, f_{rel_y} is changing sign and it becomes all negative when one of the spiral reverses the handedness. In order to identify the contributions of f_1 and f_2 to f_{rel} and f_{com}, we plot the force components for each spiral separately in appendix (Fig. E.4).

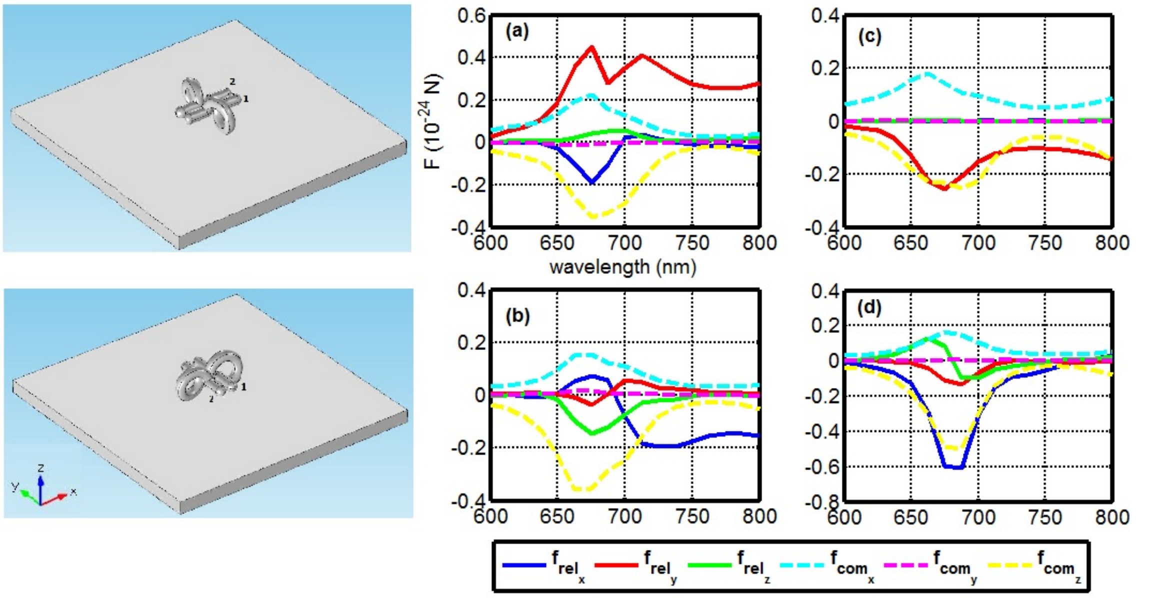

Figure 3.15: The components of the relative(solid) and common(dashed) force are plotted for two possible orientations of the rod coupled same(a,b)/cross(c,d) handed spirals above the substrate.

3.0.9 Loop coupled canonical spiral on a gold substrate

In this section, the loop coupled canonical spiral pair is placed above the gold substrate in two orientations as in the previous section. The presence of the substrate again generates f_z. We read that f_{com_z} is negative for each orientation independent of the handedness of the spirals consituting the pair (Fig. 3.16). However, f_{rel_z} is reversed from positive to negative by changing the orientation valid for either same handed or cross handed spiral pair. f_{com_x} is always positive and along the propagation direction. f_{rel_x} is attractive for same handed pairs. If the pair is replaced the cross handed one f_{rel_x} is diminished in magnitude and it also shows an asymmetric pattern crossing the zero line. Lateral force is relatively small and f_{com_y} is zero for all configuration, so the center of mass of the pairs does not feel any net force along y-axis. The relative force in y is repulsive between the spirals. The contributions from f_1 and f_2 separately to f_{rel} and f_{com} are examined in appendix (fig. E.5).

For the canonical nanospirals on the gold substrate, we can conclude that the

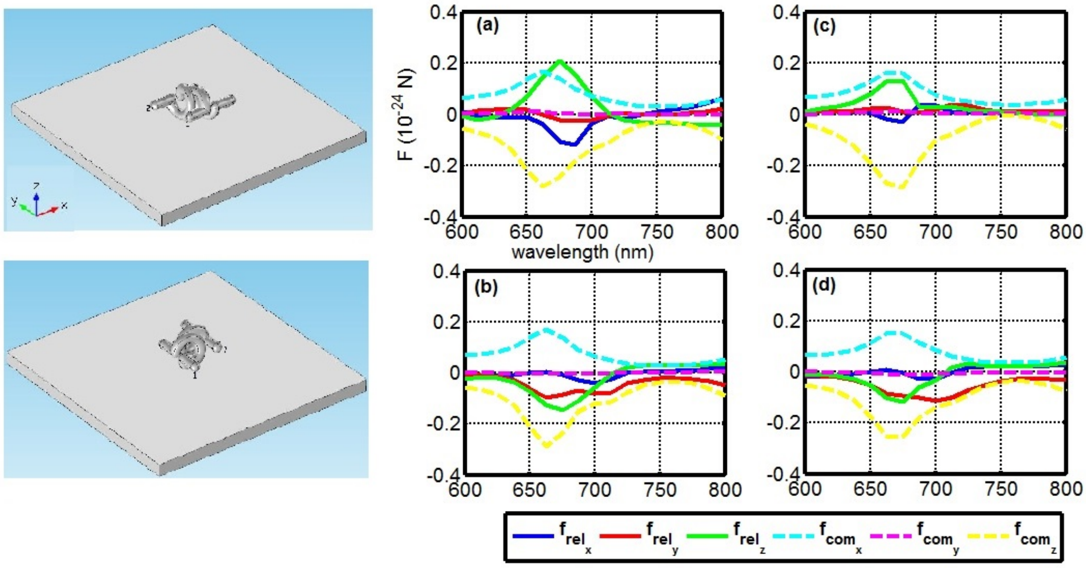

Figure 3.16: The components of the relative(solid) and common(dashed) force are plotted for two possible orientations of the loop coupled same(a,b)/cross(c,d) handed spirals above the substrate. f_{com_x} is all positive and f_{com_z} is all attractive towards the substrate. f_{com_y} reads zero.

common force along the propagation direction is comparable for all configurations. The presence of a substrate generates an attractive force on the single or coupled pair independent of its orientation. The relative force in lateral direction changes sign for rod coupled pair due to change of handedness.

Chapter 4

CONCLUSION

In this thesis, we studied the canonical spirals in microwave and optical regime. The first part of the thesis examined the electromagnetic response of the canonical-spirals in microwave whose transmission spectra were obtained both numerically and experimentally.

We conduct a systematic analysis of the electromagnetic resonant response of single canonical spirals and of the coupled canonical spiral pairs for different spatial orientations with respect to the incident linearly polarized electromagnetic wave. This enables the electric, magnetic, and electric-magnetic excitation of the resonance modes. The single spirals are designed to give the same resonance frequency, independent of excitation (polarization) and chirality. This is confirmed by measurements.

The coupled canonical spiral pairs are considered in rod-coupled and loop coupled configurations. In both coupling configurations, the splitting of the resonance of a single canonical spiral into symmetric (high frequency) and asymmetric (low frequency) modes is observed. The presence of these modes ,however, depends on the orientation of the pair as well as the chirality of the individual spirals in the pair. In particular, for rod-coupled canonical spiral pair, the symmetric mode survives for same and opposite chirality under electical excitation across the loop gap. For loop-coupled canonical pair the situation is different: symmetric (asymmetric) mode survives for opposite (same) chirality.

The final part of this study is on the transmission characteristics of one dimensional array of coupled canonical spiral pairs within a rectangular waveguide. We have found that the array generates sharp and broad band-gaps around the resonance modes of the coupled pair. Moreover, these band gaps may emerge selectively depending on the net chirality of the coupled pair, and the chirality of the neigboring spirals in adjacent pairs.

The results of the first part of the thesis indicate that the canonical spirals provide chirality dependent magnetic resonance modes under coupled configurations. These modes can be utilized for metamaterial applications to engineer effective permeability.

In the second part of the thesis, we investigate gold canonical nano-spirals having a local surface plasmon resonance at visible and near infrared part of the electromagnetic spectrum and calculate the optical force on the nano-spirals under linearly polarized light excitation. These calculations are done by electromagnetic simulations and the Maxwell stress tensor formalism of the electromagnetic force. The same systematic investigation as in the first part of the thesis work is applied starting from single canonical spirals and rod/loop coupled canonical spirals.

In the visible range, the single canonical spiral with two resonances experienced plasmonically enhanced scattering force along the propagation direction of the incident linearly polarized plane wave. The optical forces on the coupled canonical spiral pair are investigated in terms of common and relative force. The common force is acting on the center of mass of the pair, and the relative force is the mutual force between the spirals. For both loop and rod coupled pair formed either by same or cross handed canonical spirals, the common force occurs only in the propagation direction of the incident wave, as expected by the conservation of total momentum in the system. The pairs, as a whole object, are pushed along the incident plane wave. The relative lateral force reversal is achieved from attractive to repulsive by changing the handedness of a canonical spiral forming the rod coupled pair. In the loop coupled case, the reversal of the relative force from attractive to repulsive is observed in vertical direction.

When a canonical spiral or a coupled spiral pair is placed above a gold planar substrate layer, an attractive normal force towards the substrate occurs. The effect of the net chirality of the loop coupled canonical spiral pair near the substrate was negligible, but for rod coupled pair above the substrate the change in net chirality leads to the reversal of the sign of the relative lateral force.

The canonical spiral resonator can be further investigated under circularly polarized light to design metamaterials that show optical activity. Canonical spiral pairs can be utilized in biosensing applications to extend the nanorod-dimer biosensors with additional chirality-dependent functionality.

BIBLIOGRAPHY

[1] Lord Kelvin , in Baltimore Lectures on Molecular Dynamics and the Wave Theory of Light , Clay and Sons : London , 1904 , p. 449.

[2] Barron, Laurence D. Molecular light scattering and optical activity. Cambridge University Press, 2004.

[3] Rogacheva, A. V., Fedotov, V. A., Schwanecke, A. S., Zheludev, N. I. "Giant gyrotropy due to electromagnetic-field coupling in a bilayered chiral structure." Physical review letters 97.17 (2006): 177401.

[4] Pendry, J. B. "Negative refraction makes a perfect lens." Physical review letters 85.18 (2000): 3966.

[5] Smith, D. R., Padilla, W. J., Vier, D. C., Nemat-Nasser, S. C., Schultz, S. "Composite medium with simultaneously negative permeability and permittivity." Physical review letters 84.18 (2000): 4184.

[6] Pendry, J. B. "A chiral route to negative refraction." Science 306.5700 (2004): 1353-1355.

[7] Plum, E., Zhou, J., Dong, J., Fedotov, V. A., Koschny, T., Soukoulis, C. M., Zheludev, N. I. "Metamaterial with negative index due to chirality." Physical Review B 79.3 (2009): 035407.

[8] Kim, T. T., Oh, S. S., Park, H. S., Zhao, R., Kim, S. H., Choi, W., Min, B., Hess, O. "Optical activity enhanced by strong inter-molecular coupling in planar chiral metamaterials." Scientific reports 4 (2014): 5864.

[9] Zhao, R., Zhang, L., Zhou, J., Koschny, T., Soukoulis, C. M. "Conjugated gammadion chiral metamaterial with uniaxial optical activity and negative refractive index." Physical Review B 83.3 (2011): 035105.

[10] Wang, B., Zhou, J., Koschny, T., Soukoulis, C. M. "Nonplanar chiral metamaterials with negative index." Applied Physics Letters 94.15 (2009): 151112.

[11] Zhou, J., Dong, J., Wang, B., Koschny, T., Kafesaki, M., Soukoulis, C. M. "Negative refractive index due to chirality." Physical Review B 79.12 (2009): 121104.

[12] Kenanakis, G., Zhao, R., Stavrinidis, A., Konstantinidis, G., Katsarakis, N., Kafesaki, M., Economou, E. N. "Flexible chiral metamaterials in the terahertz regime: a comparative study of various designs." Optical Materials Express 2.12 (2012): 1702-1712.

[13] Zhang, S., Park, Y. S., Li, J., Lu, X., Zhang, W., Zhang, X. "Negative refractive index in chiral metamaterials." Physical review letters 102.2 (2009): 023901.

[14] Kuwata-Gonokami, M., Saito, N., Ino, Y., Kauranen, M., Jefimovs, K., Vallius, T., Svirko, Y. "Giant optical activity in quasi-two-dimensional planar nanostructures." Physical review letters 95.22 (2005): 227401.

[15] Dong, J., Zhou, J., Koschny, T., Soukoulis, C. "Bi-layer cross chiral structure with strong optical activity and negative refractive index." Optics Express 17.16 (2009): 14172-14179.

[16] Marqus, R., Medina, F., Rafii-El-Idrissi, R. "Role of bianisotropy in negative permeability and left-handed metamaterials." Physical Review B 65.14 (2002): 144440.

[17] Marqus, R., Mesa, F., Martel, J., Medina, F. "Comparative analysis of edge- and broadside-coupled split ring resonators for metamaterial design-theory and

experiments." IEEE Transactions on antennas and propagation 51.10 (2003): 2572-2581.

[18] Simovski, C. R., He, S. "Frequency range and explicit expressions for negative permittivity and permeability for an isotropic medium formed by a lattice of perfectly conducting particles." Physics letters A 311.2-3 (2003): 254-263.

[19] Huangfu, J., Ran, L., Chen, H., Zhang, X. M., Chen, K., Grzegorczyk, T. M., Kong, J. A. "Experimental confirmation of negative refractive index of a metamaterial composed of -like metallic patterns." Applied Physics Letters 84.9 (2004): 1537-1539.

[20] Ran, L., Huangfu, J. T., Chen, H. S., Li, Y., Zhang, X., Chen, K., Kong, J. A. "Microwave solid-state left-handed material with a broad bandwidth and an ultralow loss." Physical Review B 70.7 (2004): 073102.

[21] Aydin, K., Li, Z., Hudlika, M., Tretyakov, S. A., Ozbay, E. "Transmission characteristics of bianisotropic metamaterials based on omega shaped metallic inclusions." New Journal of Physics 9.9 (2007): 326.

[22] Jaggard, D. L., Mickelson, A. R., Papas, C. H. "On electromagnetic waves in chiral media." Applied physics 18.2 (1979): 211-216.

[23] Tretyakov, S. A., Mariotte, F., Simovski, C. R., Kharina, T. G., Heliot, J. P. "Analytical antenna model for chiral scatterers: Comparison with numerical and experimental data." IEEE Transactions on Antennas and Propagation 44.7 (1996): 1006-1014.

[24] Saenz, E., Semchenko, I., Khakhomov, S., Guven, K., Gonzalo, R., Ozbay, E., Tretyakov, S. "Modeling of spirals with equal dielectric, magnetic, and chiral susceptibilities." Electromagnetics 28.7 (2008): 476-493.

[25] Guven, K., Saenz, E., Gonzalo, R., Ozbay, E., Tretyakov, S. "Electromagnetic cloaking with canonical spiral inclusions." New Journal of Physics 10.11 (2008): 115037.

[26] Ashkin, A., "Acceleration and trapping of particles by radiation pressure" Phys.Rev.Lett., vol. 24, 1970.

[27] Ashkin, A., Dziedzic, J.M., Bjorkholm, J.E. and Chu,S., "Acceleration and trapping of particles by radiation pressure" Optics Letters, vol. 11, 1986.

[28] Arias-Gonzalez, J.R. and Nieto-Vesperinas, M., "Optical forces on small particles: attractive and repulsive nature and plasmon-resonance conditions" JOSA A, vol. 20, 2003.

[29] Halterman, K., Elson, J.M. and Singh, S., "Plasmonic resonances and electromagnetic forces between coupled silver nanorods" Phys.Rev.B, vol. 72, 2005.

[30] Zelenina, A.S., Quidant, R. and Nieto-Vesperinas, M., "Enhanced optical forces between coupled resonant metal nanoparticles" Optics Letters, vol. 32, 2007.

[31] Hallock, A.J., Redmond, P.L. and Brus, L.E., "Optical forces between metallic particles" PNAS, vol. 102, 2005.

[32] Liu, H., Ng, J., Wang, S.B., Hang, Z.H., Chan, C.T. and Zhu, S.N., "Strong plasmon coupling between two gold nanospheres on a gold slab" New Journal of Physics, vol. 13, 2011.

[33] Zhang, Q., Xiao, J., Zhang, X.M. and Yao, Y., "Optical binding force of gold nanorod dimers coupled to a metallic slab" Optic Communications, vol.301, 2013.

[34] Svoboda, K. and Block, S.M., "Biological Applications of Optical Forces" Annurev., 1994.

[35] Rukhlenko, I. D., Tepliakov, N. V., Baimuratov, A. S., Andronaki, S. A., Gunko, Y. K., Baranov, A. V., Fedorov, A. V. "Completely chiral optical force for enantioseparation." Scientific reports 6 (2016).

[36] Li, B., Haynie, D. T. "Chiral drug separation." Encyclopedia of chemical processing 1 (2006): 449-58.

[37] Chhabra, N., Aseri, M. L., Padmanabhan, D. "A review of drug isomerism and its significance." International Journal of Applied and Basic Medical Research 3.1 (2013): 16.

[38] Ding, K., Ng, J., Zhou, L., Chan, C. T. "Realization of optical pulling forces using chirality." Physical Review A 89.6 (2014): 063825.

[39] Alizadeh, M. H., Reinhard, B. M. "Plasmonically enhanced chiral optical fields and forces in achiral split ring resonators." ACS Photonics 2.3 (2015): 361-368.

[40] Zhao, Y., Saleh, A. A., Dionne, J. A. "Enantioselective optical trapping of chiral nanoparticles with plasmonic tweezers." ACS Photonics 3.3 (2016): 304-309.

[41] Tkachenko, G., Brasselet, E. "Optofluidic sorting of material chirality by chiral light." Nature communications 5 (2014).

[42] Canaguier-Durand, A., Hutchison, J. A., Genet, C., Ebbesen, T. W. "Mechanical separation of chiral dipoles by chiral light." New Journal of Physics 15.12 (2013): 1230

[43] Hayat, A., Mueller, J. B., Capasso, F. "Lateral chirality-sorting optical forces." Proceedings of the National Academy of Sciences 112.43 (2015): 13190-13194.

[44] Alizadeh, M. H., Reinhard, B. M. "Transverse chiral optical forces by chiral surface plasmon polaritons." ACS Photonics 2.12 (2015): 1780-1788.

[45] Wang, S. B., Chan, C. T. "Lateral optical force on chiral particles near a surface." Nature communications 5 (2014).

[46] Aydin, K., Ozbay, E. "Experimental and numerical analyses of the resonances of split ring resonators." physica status solidi (b) 244.4 (2007): 1197-1201.

[47] Zhao, R., Tassin, P., Koschny, T., Soukoulis, C. M. "Optical forces in nanowire pairs and metamaterials." Optics express 18.25 (2010): 25665-25676.

[48] Penciu, R. S., Aydin, K., Kafesaki, M., Koschny, T., Ozbay, E., Economou, E. N., Soukoulis, C. M. "Multi-gap individual and coupled split-ring resonator structures." Optics express 16.22 (2008): 18131-18144.

[49] https://www.comsol.com/

[50] Johnson, P.B. and Christy, R.W., "Optical constants of the noble metals" Phys.Rev.B, vol. 6, 1972.

[51] Nieto-Vesperinas, M., Senz, J. J., Gmez-Medina, R., Chantada, L. "Optical forces on small magnetodielectric particles." Optics express 18.11 (2010): 11428-11443.

[52] Jackson, "Classical Electrodynamics, 2nd edition" (John Wiley Sons)

Appendix A

THE MAXWELL STRESS TENSOR

Both the gradient and scattering type optical forces can be calculated using the Maxwell stress tensor formalism. In the following, we briefly present the derivation of the Maxwell's stress tensor starting from Maxwell's equations and formulate the optical force, as can be found in standard electrodynamics textbooks [52].

$$\nabla \cdot \mathbf{E} = 4\pi\rho \tag{A.1}$$

$$\nabla \cdot \mathbf{B} = 0 \tag{A.2}$$

$$\nabla \times \mathbf{E} = -\frac{1}{c}\frac{\partial \mathbf{B}}{\partial t} \tag{A.3}$$

$$\nabla \times \mathbf{B} = \frac{4\pi}{c}\mathbf{j} + \frac{1}{c}\frac{\partial \mathbf{E}}{\partial t} \tag{A.4}$$

From the Lorentz force, we can define the force density f, then total force in a volume V will be

$$\mathbf{f} = \rho\mathbf{E} + \frac{1}{c}\mathbf{j} \times \mathbf{B} \tag{A.5}$$

$$\mathbf{F} = \int_V [\rho\mathbf{E} + \frac{1}{c}\mathbf{j} \times \mathbf{B}]dV \tag{A.6}$$

We can eliminate ρ and $\mathbf{j}$ using Maxwell equations(1st and 4th)

$$\mathbf{f} = \frac{1}{4\pi}[\mathbf{E}(\nabla \cdot \mathbf{E}) + \frac{1}{c}\mathbf{B} \times \frac{\partial \mathbf{E}}{\partial t} - \mathbf{B} \times (\nabla \times \mathbf{B}) \tag{A.7}$$

Now, we can write that

$$\frac{\partial}{\partial t}(\mathbf{E} \times \mathbf{B}) = \left(\mathbf{E} \times \frac{\partial \mathbf{B}}{\partial t}\right) - \left(\mathbf{B} \times \frac{\partial \mathbf{E}}{\partial t}\right) \tag{A.8}$$

and we obtain

$$\mathbf{f} = \frac{1}{4\pi}[\mathbf{E}(\nabla \cdot \mathbf{E}) + \mathbf{B}(\nabla \cdot \mathbf{B}) - \mathbf{E} \times (\nabla \times \mathbf{E}) - \mathbf{B} \times (\nabla \times \mathbf{B})] - \frac{1}{4\pi c}\frac{\partial}{\partial t}(\mathbf{E} \times \mathbf{B}) \tag{A.9}$$

The i^{th} component of the following expression can be written as

$$[\mathbf{E}(\nabla \cdot \mathbf{E}) - \mathbf{E} \times (\nabla \times \mathbf{E}]_i = \sum_j \frac{\partial}{\partial j}(E_i E_j - \frac{1}{2}\mathbf{E} \cdot \mathbf{E}\delta_{ij}) \tag{A.10}$$

At this stage we introduce the Maxwell's stress tensor as follows

$$T_{i\,j} = \frac{1}{4\pi}[(E_i E_j - \frac{1}{2}\delta_{i\,j}E^2) + (B_i B_j - \frac{1}{2}\delta_{i\,j}B^2)] \tag{A.11}$$

where $\delta_{i\,j}$ is the Kronecker delta and the indices i, j are space coordinates (x, y, z). Force per unit volume can be written as

$$\mathbf{f} = \nabla \cdot \overleftrightarrow{\mathbf{T}} - \frac{1}{4\pi c}\frac{\partial}{\partial t}(\mathbf{E} \times \mathbf{B}) \tag{A.12}$$

Then the total force on the charges in the volume V is given by

$$\mathbf{F} = \int_V \nabla \cdot \overleftrightarrow{\mathbf{T}} dV - \frac{1}{4\pi c}\frac{d}{dt}\int_V (\mathbf{E} \times \mathbf{B}) dV \tag{A.13}$$

The volume integral of the first term can be converted to a surface integral using the divergence theorem, so the mechanical force is equal to

$$\mathbf{F} = \oint_{\partial V} \overleftrightarrow{\mathbf{T}} \cdot \mathbf{n} da - \frac{1}{4\pi c}\frac{d}{dt}\int_V (\mathbf{E} \times \mathbf{B}) dV \tag{A.14}$$

where ∂V denotes the surface enclosing the volume V, $\mathbf{n}$ is the unit vector perpendicular to the surface, da is the infinitesimal area element, and the second term of the equation 2.14 is proportional to the Poynting vector $\mathbf{S} = \frac{c}{4\pi}(\mathbf{E} \times \mathbf{H})$.

We can show also the conservation of momentum starting with the Newton's second law

$$\mathbf{F} = \frac{d\mathbf{p}_{mech}}{dt} \tag{A.15}$$

, then we write

$$\frac{d\mathbf{p}_{mech}}{dt} = \oint_{\partial V} \overleftrightarrow{\mathbf{T}} \cdot \mathbf{n} da - \frac{1}{4\pi c}\frac{d}{dt}\int_V (\mathbf{E} \times \mathbf{B}) dV \tag{A.16}$$

where $\mathbf{p}_{mech}$ is the mechanical momentum of the particles contained in volume V. The second term of the right-hand-side of the expression is the field momentum, which is the momentum carried by electromagnetic fields.

$$\mathbf{p}_{field} = \frac{1}{4\pi c}\int_V (\mathbf{E} \times \mathbf{B})dV \tag{A.17}$$

Hence, total momentum which is the sum of the mechanical and field momentum can be written as

$$\frac{d}{dt}[\mathbf{p}_{mech} + \mathbf{p}_{field}] = \oint_{\partial V} \overleftrightarrow{\mathbf{T}} \cdot \mathbf{n}da \tag{A.18}$$

For time-harmonic fields, the average of the field momentum term over one oscillation period vanishes. The remaining expression for the time-averaged force is

$$\langle \mathbf{F} \rangle = \oint_{\partial V} \langle \overleftrightarrow{\mathbf{T}} \rangle \cdot \mathbf{n}da \tag{A.19}$$

$\overleftrightarrow{\mathbf{T}}$ is actually the force per unit area acting on the surface, and the diagonal elements represent pressures and off-diagonal elements represent shears. Equation 2.20 allows one to calculate the mechanical force on a body within the closed surface. The force is determined by the electric and magnetic fields on the surface ∂V.

For macroscopic media, the field momentum density $\mathbf{g}$ and the Maxwell stress tensor is

$$\mathbf{g} = \frac{1}{4\pi c}(\mathbf{E} \times \mathbf{H}) \tag{A.20}$$

$$T_{ij} = \frac{1}{4\pi}[E_i D_j - \frac{1}{2}\delta_{ij}(\mathbf{E} \cdot \mathbf{D}) + H_i B_j - \frac{1}{2}\delta_{ij}(\mathbf{B} \cdot \mathbf{H})] \tag{A.21}$$

The medium is assumed to be linear, but it is not necessary to be isotropic in i-direction. There is no restriction in size (except few atoms sizes) and shape of the body, as to its dielectric properties. This method is widely applicable, such as for purely electric, purely magnetic or fully electromagnetic effects, and for traveling or evanescent wave fields.

Appendix B

FORCE EXERTED ON A CHIRAL DIPOLE

The optical forces on a small particle in a source-free, lossless, nondispersive, and isotropic medium with relative electric permittivity ϵ and relative magnetic permeability μ. In the dipole approximation, the time-averaged total optical force F exerted on the particle by a monochromatic electromagnetic wave is given by ([51, 43]):

$$\mathbf{F} = \frac{1}{2} Re\{\mathbf{d}(\nabla \otimes \mathbf{E}^*) + \mathbf{m}(\nabla \otimes \mathbf{H}^*)\} - \frac{k^4}{3} Re\{\sqrt{\frac{1}{\mu\epsilon}}(\mathbf{d} \times \mathbf{m}^*)\} \tag{B.1}$$

where $\otimes$ is dyadic product and * denotes complex conjugate. k is the wavenumber given b $k = n\omega/c$, where ω is the frequency, c speed of light in vacuum and $n = \sqrt{\epsilon\mu}$ the refractive index of the medium.

The electric and magnetic dipole moments $(\mathbf{d}, \mathbf{m})$ of a chiral particle due to incident fields, assuming that the polarizabilities are isotropic, are

$$\mathbf{d} = \alpha_e \mathbf{E} + i\chi \mathbf{H} \tag{B.2}$$

$$\mathbf{m} = \alpha_m \mathbf{H} - i\chi \mathbf{E} \tag{B.3}$$

where are α_e and α_m electric and magnetic polarizabilities and χ is the chiral polarizability. When electric and magnetic dipole moments are inserted in equation B.1, the full expression of the optical force applied on a chiral dipole is given as ([43])

$$\mathbf{F}_0 = \frac{1}{g}(\frac{1}{\epsilon} Re\{\alpha_e\} \nabla u_e + \frac{1}{\mu} Re\{\alpha_m\} \nabla u_m) - \frac{\omega}{g} Re\{\chi\} \nabla h \tag{B.4}$$

$$+\frac{2\omega}{g}(\mu Im\{\alpha_e\} \mathbf{p}_e^o + \epsilon Im\{\alpha_m\} \mathbf{p}_m^o) - \frac{c}{g} Im\{\chi\}[\nabla \times \mathbf{p} - 2k^2 \mathbf{s}] \tag{B.5}$$

$$\mathbf{F}_{int} = \frac{2\omega}{g}\frac{k^3}{3}(Re\{\alpha_e\alpha_m^*\}\mathbf{p} - Im\{\alpha_e\alpha_m^*\}\mathbf{p}" + |\chi|^2\mathbf{p}] \tag{B.6}$$

$$-\frac{2\omega}{g}\frac{2k^4}{3n}(\epsilon Re\{\chi\alpha_m^*\}\mathbf{s}_m + \mu Re\{\chi\alpha_e^*\}\mathbf{s}_e) \tag{B.7}$$

The expression is given in Gaussian units, $g = 1/(4\pi)$, $u_e = (g\epsilon/4)|\mathbf{E}|^{\mathbf{2}}$ and $u_m = (g\mu/4)|\mathbf{H}|^{\mathbf{2}}$ are electric and magnetic energy density and time-averaged optical helicity density $h = (g/2\omega)Im\{\mathbf{E}\cdot\mathbf{H}^*\}$. $\mathbf{p}$ is the time-averaged Poynting momentum density $\mathbf{p} = (g/2c)Re\{\mathbf{E}\times\mathbf{H}^*\}$ and $\mathbf{p}$" is the imaginary part of hte Poynting momentum density. p is formed by p^o related to orbital angular momentum and Belifante momentum density p^s related to the spin momentum density $\mathbf{s}$ as sum of $\mathbf{s_e}$ and $\mathbf{s_m}$.

$$\mathbf{p^s} = -\frac{g}{8\omega}\nabla\times[\frac{1}{i\mu}\mathbf{E}\times\mathbf{E}^* + \frac{1}{i\epsilon}\mathbf{H}\times\mathbf{H}^*] \tag{B.8}$$

$$\mathbf{p^o} = -\frac{g}{4\omega}Im\{\frac{1}{\mu}\mathbf{E}(\nabla\otimes\mathbf{E}^*) + \frac{1}{\epsilon}\mathbf{H}(\nabla\otimes\mathbf{H}^*)\} \tag{B.9}$$

$$\mathbf{s} = \frac{g}{4\omega}(\frac{1}{i\mu}\mathbf{E}\times\mathbf{E}^* + \frac{1}{i\epsilon}\mathbf{H}\times\mathbf{H}^*) \tag{B.10}$$

The first two terms of $\mathbf{F_0}$ written B.4 is the gradient force term and last two terms named B.5 are radiation pressure which are familiar expression in the case of achiral dipole, $\chi = 0$. $\mathbf{F_{int}}$ is the consequence of the interaction of the electric and magnetic dipole moments.

For a plane wave propagating in x direction, the forces are along the propagation direction as given

$$\mathbf{F_0} = [(Im\{\mu\alpha_e\} + Im\{\epsilon\alpha_m\})/2]Ik\hat{\mathbf{x}} \tag{B.11}$$

$$\mathbf{F_{int}} = [Re\{\alpha_e\alpha_m^*\} + |\chi|^2]Ik^4/3\hat{\mathbf{x}} \tag{B.12}$$

where $I = n^{-1}|\mathbf{E}\times\mathbf{H}^*|$.

Appendix C

CANONICAL SPIRALS IN MICROWAVE REGIME

The simulations are performed in CST Microwave Studio. The steps basically are constructing the geometry, setting material of the components, defining the boundary conditions and the frequency range, selecting the solver and djusting the mesh. The resonance of the single spiral is examined in a rectangular computational domain by using ports as the excitation source with perfect electric conductor (PEC) and perfect magnetic conductor (PMC) boundary conditions.

The orientations of the canonical spiral corresponding the reverse boundary conditions inside the waveguide give the same resonance frequency.

Furthermore, in simulations using the unit cell boundary conditions which simulate a metamaterial constituted by the spirals, the same resonance behaviour is obtained, even the cross-polarized electric field component is obtained reproducing the study in ref. [24].

We further change the geometrical parameters of the canonical spiral in order to match the experimental results. The new design parameters are adjusted such that still the electromagnetic response of RH/LH spiral is the same for TE and TM polarizations.

The fabrication of the canonical spirals are done simply by hands. A piece of solder wire of length equal to the total length of the flattened spiral design is wrapped around a stick. Further adjustments for the length of the straigth segments and the gap distance are completed by measuring the response of the spiral inside the waveguide until matching the desired resonance frequency.

Appendix D

COMPUTATIONAL PROCEDURE IN OPTICAL REGIME

We employ Comsol Multiphysics, which is a finite element software, to solve the scattering problem of the subwavelength metallic particle illuminated by a plane wave.

We perform a 3D simulation. The geometry is constructed for the vacuum case. The nanostructure's center of mass is placed at the origin of a large spherical computational domain where the most outer layer is chosen to be a perfectly matched layer (PML). PML is a layer absorbing the incident radiation on it without creating reflections from the boundary. PML is absorbing radiation coming from wide range of incidence angles. The size of the computational domain is set to be equal to one half of the excitation wavelength, so that the computational size is adjusted with respect to the excitation wavelength in order to reduce memory and execution time.

For reducing the computational memory, the mesh is defined differently on the domains with different sizes and materials. The maximum mesh size for the domains except the nanostructures, are one sixth of the wavelength. For the nanostructures, a much refined mesh is selected.

THz frequencies corresponding to a wavelength range 600-1300 nm are studied. We employ a parametric sweep node under the frequency domain study. The incident plane wave is given as an input for the background electric field under the "electromagnetic waves" node which solves for the scattered field. The electric field polarized along the z-axis is given as $E_0 exp(-jk_0 x)$, where k_0 is the vacuum wave vector.

Gold permittivity values are taken from the Johnson and Christy [50] and interpolated to construct a frequency dependent dielectric function in the relevant frequency range.

The optical force calculations are done on the surface defined as a helix and a cylinder with hemispherical caps encapsulating each nanorod separately. Theoretically, any integration surface should work, such as a simple cylinder or rectangular box. However we experienced numerical difficulties due to the discontinuities at the box edges, hence a smooth surface is better for numerical purposes. The force calculation can be done directly on the canonical spiral. However, as mentioned in ref. [47], we need an integration surface where all fields are well-defined. We verify this requirement by calculating the force components on the surface of the canonical spiral. We see that the all forces are exactly equal to zero. Again the mesh is carefully designed between the canonical spiral surface and the integration surface.

Appendix E

OPTICAL FORCES ON CANONICAL SPIRALS

E.1 Optical forces on rod coupled canonical spirals

In this section, we show the optical force components for a rod coupled pair composed of opposite handed spirals.The findings for each orientations A-F are as follows : Fig. E.1.A exhibits same f_{1x}, f_{2x} both in direction(sign) and magnitude, f_{1y}, f_{2y} are zero, and f_{1z}, f_{2z}, which are stronger with respect to f_x are different in sign, possessing the same magnitude. For the orientation B, f_{z1}, f_{z2} are zero, $f_{x_{1,2}}$ have same magnitude and sign. f_{y2} has positive sign, whereas f_{y1} has negative sign. In C, both spirals do not feel any force in y,z direction. The scattering force differs for spiral 1 and 2, and it is positive in the studied range of wavelength. In D, the spirals are symmetrically positioned about the propagation of the incident wave, which exerts same magnitude and direction f_x on each spiral. $f_{z1,2}$ are zero. In E, f_y, f_z are calculated to be nearly zero, only f_x along propagation direction is noted, which is negative for $spiral_1$, positive for $spiral_2$, around 660 nm.

E.2 Optical force on loop coupled canonical spiral pair

The optical force components on the loop coupled pair composed of same and cross handed spirals are plotted in Fig. E.2 and Fig. E.3 respectively.

- A.f_{x1} and f_{x2} are not the same in contrary to rod coupled spirals, since in order to position loop on loop there is a misalignment along propagation direction. f_z reverses sign and f_{z1}, f_{z2} behaves in opposite sense. f_{rel_z} become repulsive to attractive after saddle point around 690 nm. f_y is calculated to be really small having opposite sign for each spiral.

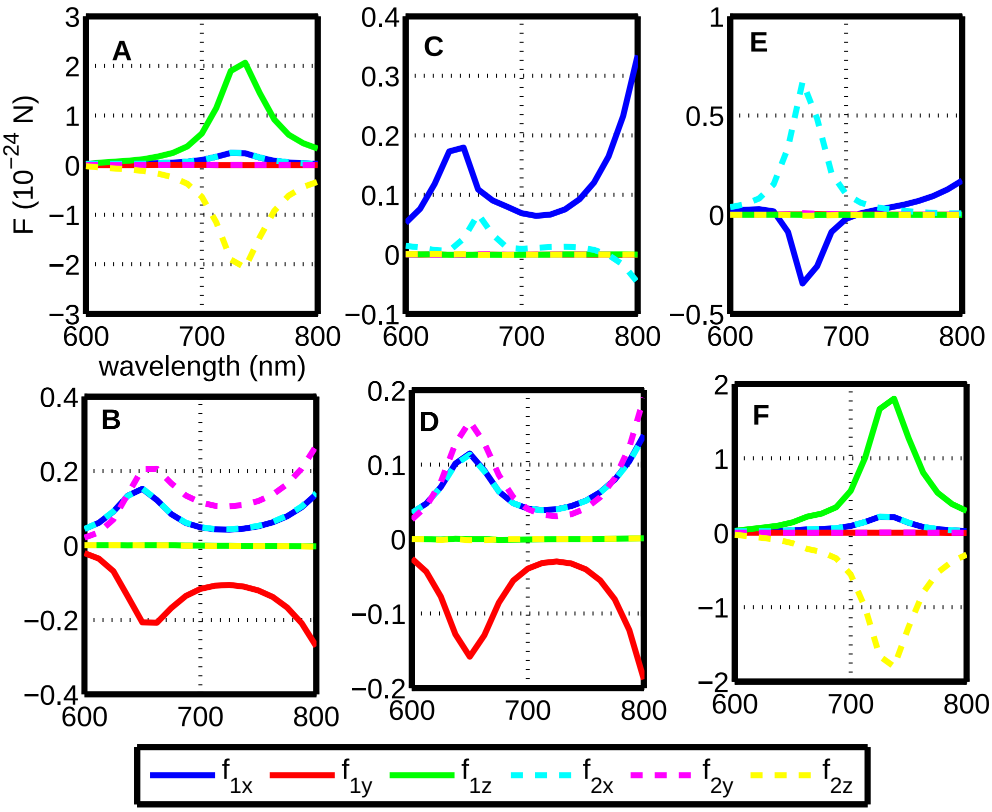

Figure E.1: The optical force components f_x, f_y, f_z spectra of the cross handed rod coupled canonical spirals, seperately for spiral1,2, in orientations A-F are plotted.

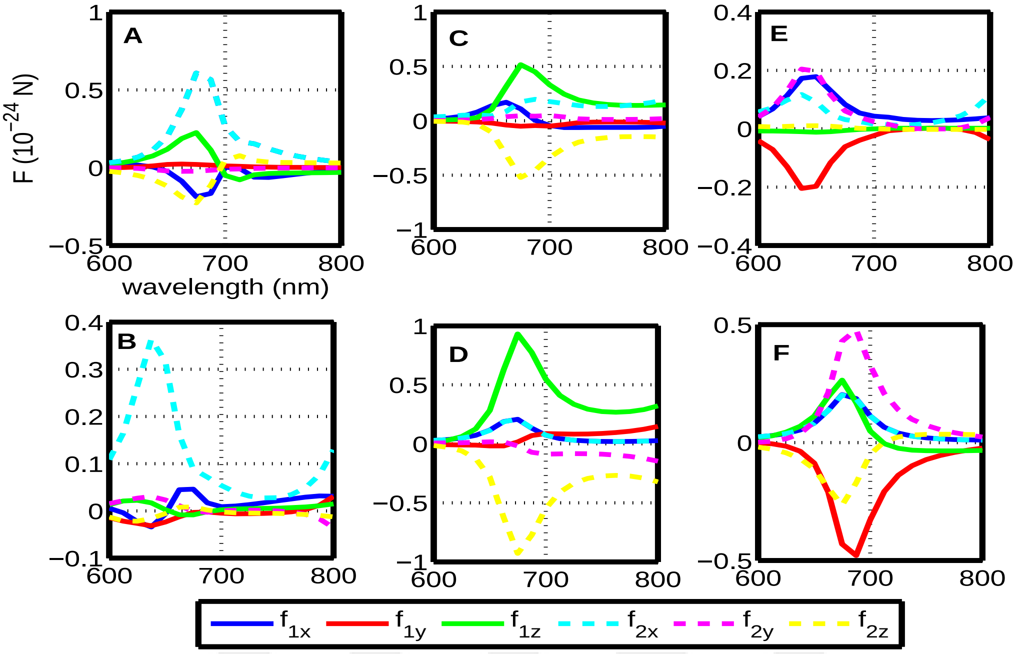

Figure E.2: The optical force components spectra of the same handed loop coupled canonical spirals in orientations A-F are plotted.

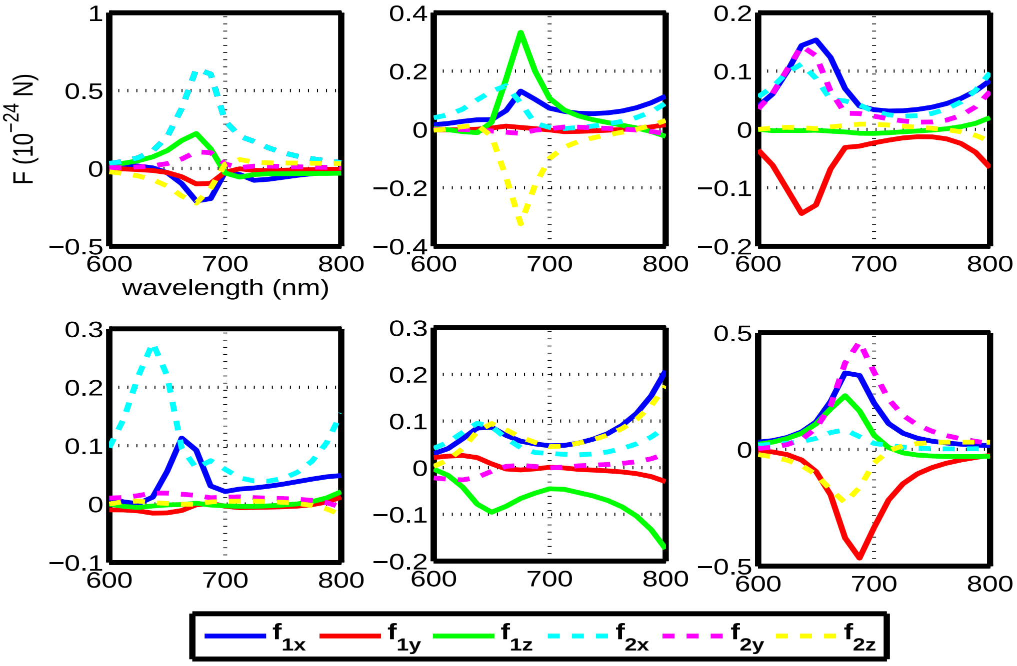

Figure E.3: The optical force components spectra of the opposite handed loop coupled canonical spirals in orientations A-F are plotted.

- B. f_{2x} shows similar behaivour as in A, but the peak shifted to lower wavelength of 640 nm.

- C. f_{2x} is all positive, but f_1x changes sign. small relative repulsivef_y. The attractivef_{rel_z} is stronger than other force components.

- D. The symmetric incidence of the plane wave results in same $f_{x1,2}$. So f_{rel_x} is zero, f_{com_x} shows that the spiral pair together pushed along the propagation.

- E. The dominant force component is f_y. f_x is positive, but different in magnitude for spiral1,2

E.3 Optical forces on coupled canonical spirals above the substrate

The rod coupled canonical spiral pair is placed 7.5 nm above the gold substrate. Two possible orientations are examined, where rods are along the propagation direction and the gap are asymmetric to the electric field, and rods are parallel to the magnetic field and the gap is symmetric to the propagation vector. In fig. E.4.a,c plots each force component for each same handed spiral in two different orientations, in fig. E.4.b,d plots each force component for cross handed spiral.

Fig. E.5.a,c plots each force component for same handed spiral pair in two different orientations, where the spirals are loop coupled, in fig. E.5.b,d plots each force component for cross handed spiral.

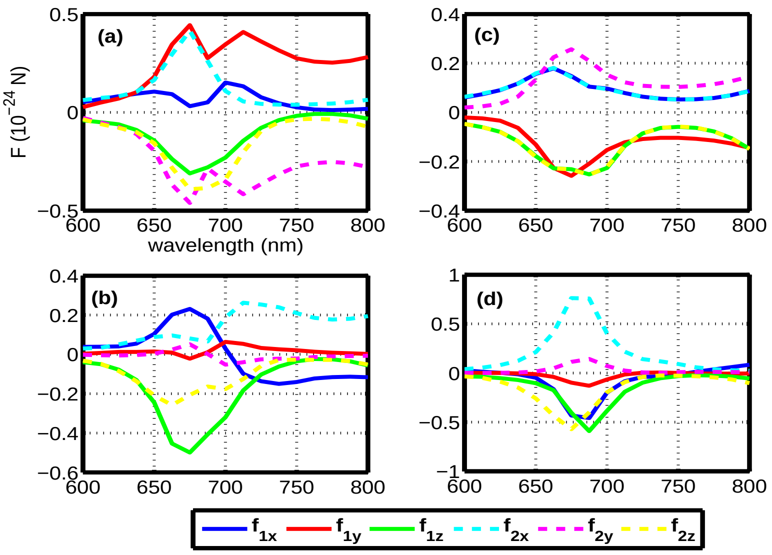

Figure E.4: Spectra of $f_{x,y,z}$ on $spiral_1$ and $spiral_2$ are plotted for two possible orientations of the rod coupled same handed spirals (a,b) and cross handed spirals (c,d) above the substrate.

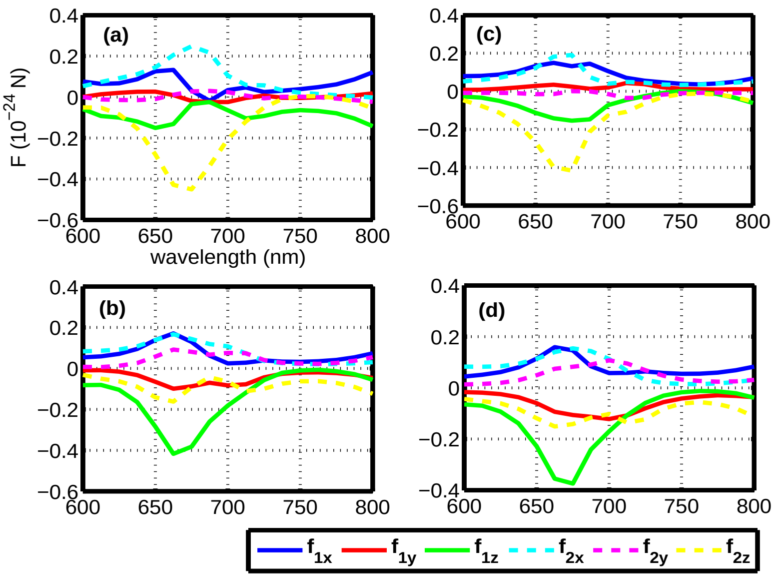

Figure E.5: Spectra of $f_{x,y,z}$ on spiral 1 and spiral 2 are plotted for two possible orientations of the loop coupled same handed spirals (a,b) and cross handed spirals (c,d) above the substrate.